



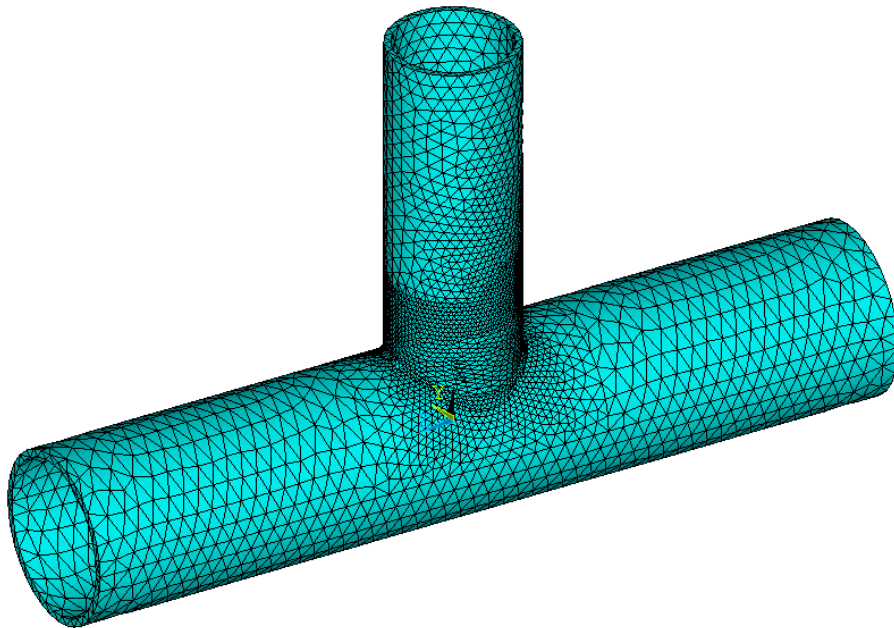
M Ű E G Y E T E M 1 7 8 2

Szakály Ferenc

Student, MSc in Computational Structural Engineering, BUTE (M.Sc.)

Deterministic and stochastic investigation of welded,
high strength steel T joint

Scientific Student's Association Thesis



Supervisor:

Dr. Vigh László Gergely

Department of Structural Engineering, BUTE

Budapest, 2013

Table of contents

1. Introduction	1
1.1. Background, motivation	1
1.2. Problem statement, aims.....	1
1.3. Solution strategy	1
2. Literature review	2
2.1. Laboratory experiments.....	2
2.2. Failure modes.....	2
2.3. Numerical analyses	4
2.4. Design methods.....	6
3. Design method according to the EC3-1-8	7
3.1. Review on the design of T joints according to the Eurocode.....	7
3.1.1. <i>Geometric restrictions</i>	7
3.1.2. <i>Design formulae</i>	8
3.2. Design resistances of the investigated T joints according to the standard.....	10
3.2.1. <i>Checking of the geometric constraints for the first assembly</i>	11
3.2.2. <i>Determine the static resistances for the first assembly</i>	12
3.2.3. <i>Tabulated results for all the assemblies</i>	15
4. Numerical modelling technique	19
4.1. Development of the geometry.....	19
4.1.1. <i>Joint geometry</i>	19
4.1.2. <i>Modelling of the weld</i>	20
4.1.3. <i>Applied material model</i>	21
4.2. Convergence test, the finite element mesh generation.....	22
4.3. Boundary conditions	24
4.4. Validation of the finite element model.....	26
5. Development of design formulation	29
5.1. Parametric simulations	29
5.1.1. <i>Analysis methodology</i>	29
5.1.2. <i>Results for the first assembly</i>	29
5.1.3. <i>Tabulated results for all the assemblies</i>	32
5.2. Modification of the design formulae.....	34
5.2.1. <i>Axial resistance</i>	34

5.2.2. <i>In plane bending resistance</i>	36
6. Design method calibration	39
6.1. Stochastic modelling	39
6.2. Determination of the necessary repetition number	39
6.3. Identification of the safety factor	43
6.3.1. <i>Partial safety factor for the first assembly</i>	43
6.3.1. <i>Tabulated results for all the assemblies</i>	44
7. Conclusions	46
8. References	47

1. Introduction

1.1. Background, motivation

Nowadays, especially in the field of bridge construction there is an increasing interest about the high strength steels (HSS), but the current European standard does not provide the sufficient basis to promote the spread of its application. The hollow sections are frequently used both at the territory of bridge and building construction, due to their good structure forming capabilities and easy assembly. In this study, firstly the brief review of design recommendations on these structures is considered, taking into account the restrictions coming from the application of HSS and the current research directions. After that the main purpose is to develop such design formulae, which –keeping the adequate level of safety -lead to more economical results, based on series of relevant numerical simulations.

1.2. Problem statement, aims

In the third Eurocode, the part 1-8 contains the design formulae correspond to the hollow section joints, but in many cases they result in a very conservative solution, especially with the prescriptions of HSSs, according to the part 1-12. Because of the continuously increasing interest on this area, from economical point of view a less conservative design methodology would be highly beneficial. Unfortunately, the number of experiments on HSS steels are very low, and at the majority of the cases they focus on the fatigue behaviour instead of the static resistance, which is also valid for hollow section joint experiments, where in addition the sections are usually filled by concrete. These reasons lead to the necessity of the detailed static investigation of HSS hollow section joints, which involves the accuracy of the standard design formulae.

1.3. Solution strategy

For the mentioned purpose, after the review of the design recommendations I develop a parametric finite element model, which must be validated according to real experiments to obtain relevant results. During the numerical simulations, both axial and bending loads will be considered, and for several assemblies - covering a large field of applicable CHS sections - I determine the load-bearing capacity of the joint. By the comparison of the numerical and standard results, I suggest modified formulae for the characteristic value of the static resistances. After that, by taking into account the material and geometrical uncertainties, I perform Monte-Carlo simulations to determine a partial safety factor for the new resistance formulae, and compare the final results with the Eurocode.

2. Literature review

2.1. Laboratory experiments

Nowadays, in those studies which investigate the static behaviour, usually the results of quite old tests are used for the validation of the numerical model, performed in the previous century. The present laboratory experiments are mainly concentrates on the examination of the fatigue behaviour, the stress distribution around the weld. The other group of the experiments is investigate the mechanical response of the concrete filled sections, where the static and fatigue resistance are both considered. In this study, the utilized experimental results are the part of a very large test series, which was conducted between 1964 and 1991, resulted in a valuable tubular joint database (Lesani, Bahaari, & Shokrieh, 2013). At these tests, the geometry of the specimen, the material properties and load-bearing capacity were recorded, thus these will be the initial data for the validation.

2.2. Failure modes

Generally, in case of hollow section joints the EC distinguish six types of failure modes (Eurocode 3 EN 1993-1-8:2005 (E), 2005), the *chord face failure [a]*, the *chord side wall failure [b]*, the *chord shear failure [c]*, the *punching shear failure [d]*, the *brace failure [e]* and *local buckling [f]* (Figure 2.2). If we keep the prescribed geometric restrictions, only two failure modes should be considered, the *chord face failure* and the *punching shear failure*, beside the individual failure of the brace or chord. These modes can be seen on (Figure 2.1), where on the left figure instead of a T a K joint is represented, but it reflects very well the characteristics of this failure.

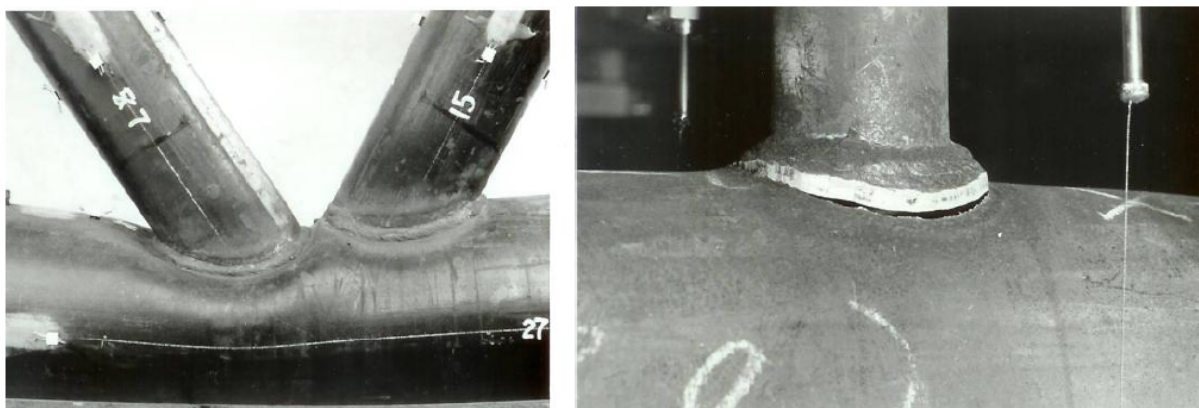


Figure 2.1. Chord face failure (left) and punching shear failure (right) of hollow section joints (Wardenier, Kurobane, Packer, Vegte, & Zhao, 2008)

The *chord face failure* is the most usual failure mode for joints with a single bracing such as T-joints, and in case of K and N joints with a gap between the bracings if the bracing to chord width ratio is less than 0.85 (Tata Steel, 2011). It is practically the plastification of the chord cross-section. The *punching shear failure* usually caused by a crack initiation in the chord face, leading to the rupture of the chord. Generally it is not typical, only in the case when the chord width to thickness ratio is relatively small. Both failure modes can be the result of axial or (in plane or out of plane) moment loading, or of course the combination of them.

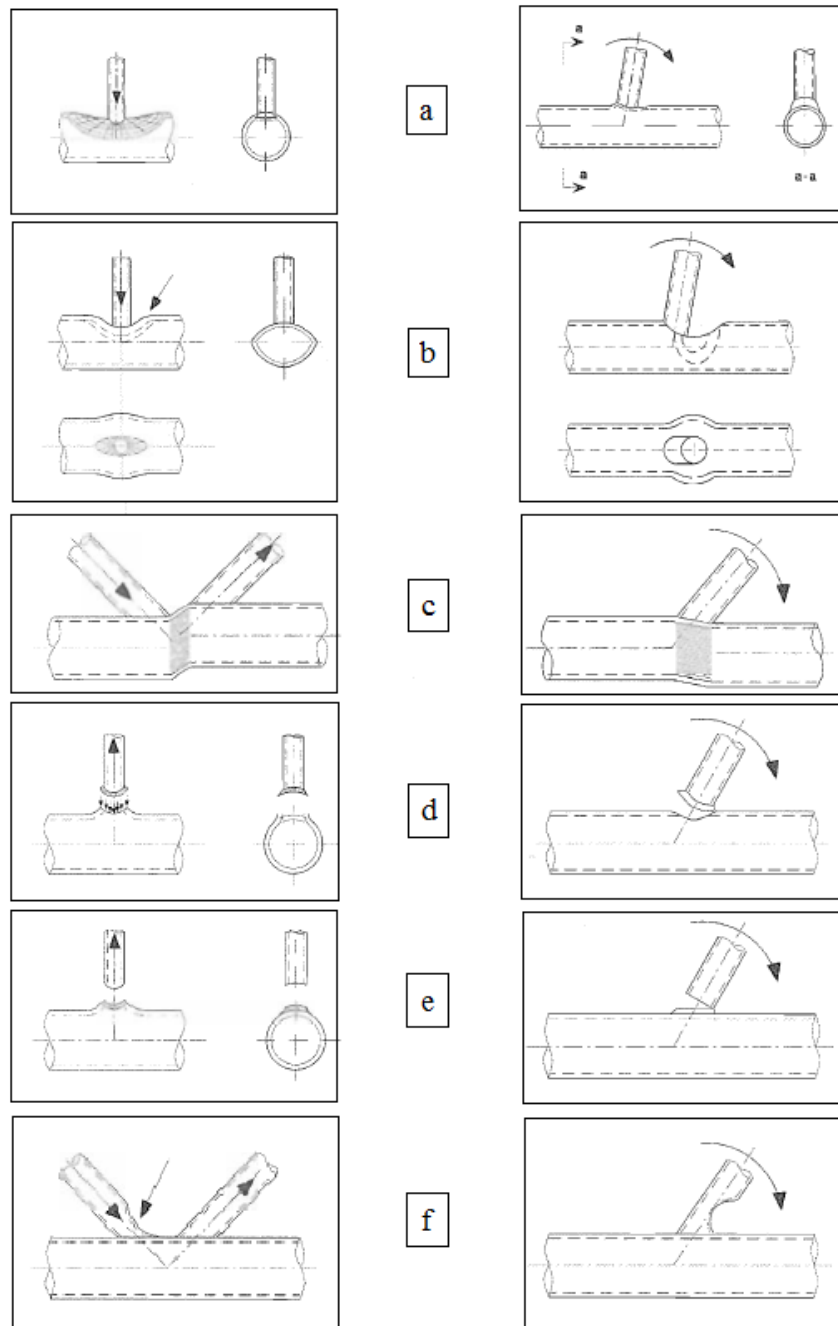


Figure 2.2. The different failure modes of hollow section joints in general case
(Eurocode 3 EN 1993-1-8:2005 (E), 2005)

2.3. Numerical analyses

In the earlier decades, for the main failure modes (*Chapter 2.2*) different resistance models were developed based on mechanical simplifications and laboratory experiments. A typical example for this is the study of (H.S.Mitri, 1988), where the in plane moment resistance of tubular T and Y joints was investigated. As the *punching shear* is the typical failure for this loading case, a model for this have been built, where the yield stress developing through the thickness of the chord is equilibrated by the bending moment (*Figure 2.3*). It is worth to mention that the current EC formula is also based on this approach. After the model formulation, they compared the received results with the available laboratory results, taken from different database.

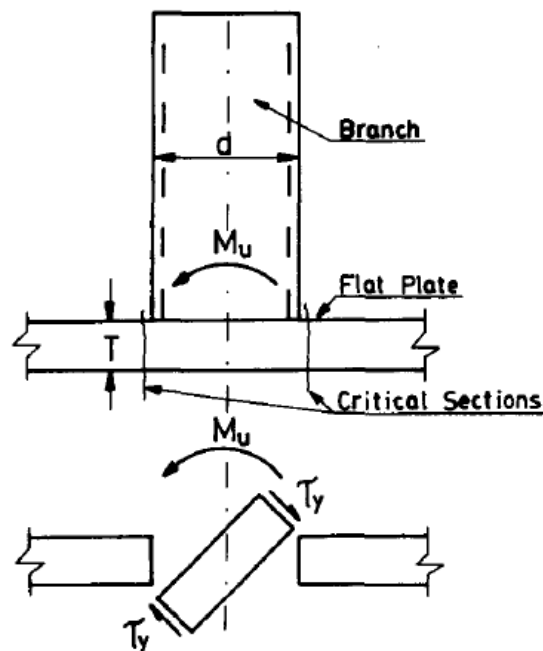


Figure 2.3. *Punching shear model for in plane bending (H.S.Mitri, 1988)*

Similarly to the previous simplified model, for the *chord plastification* the so called ring model was introduced, firstly in 1967 (Wardenier, Packer, Zhao, & Vegte, 2010). This model is based on the assumption that most of the loads is transferred at the saddles of the brace, since the chord is stiffer at these parts on the perimeter, thus here the stresses significantly larger comparing to the middle parts of the chord. According to (*Figure 2.4*), it is assumed that the axial load on the brace is transferred to the chord as two concentrated forces. At the development of the design formula, they calculated the plastic moment capacity (according to the model at point A and B the moment reaches this limit value), which was equilibrated by the bending moment coming from the axial forces at the saddles of the brace.

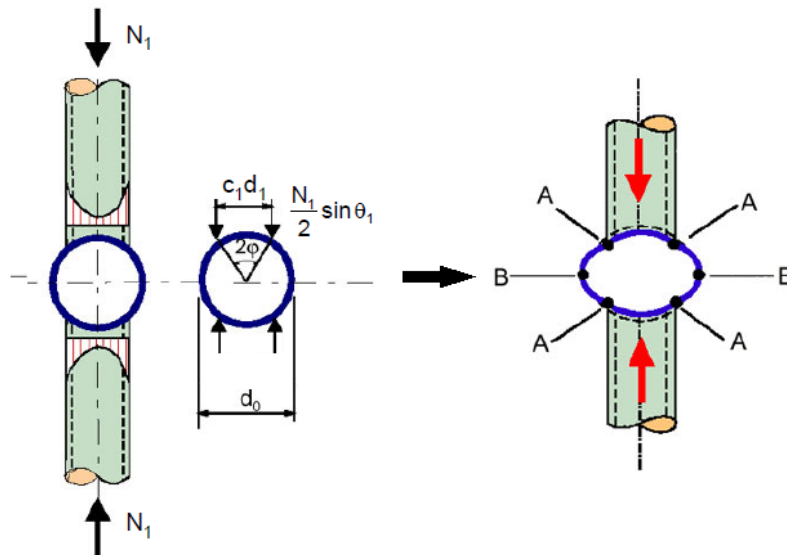


Figure 2.4. The ring model developed for the chord plastification
(Wardenier, Kurobane, Packer, Vegte, & Zhao, 2008)

In the recent past, (Lesani, Bahaari, & Shokrieh, 2013) presented their work about T and Y joints subjected to axial compressive loads. Here a parametric model, made of shell elements was developed to investigate the behaviour of the connection. Here, the angle between the brace and chord varied between 30° to 90° , and for the different geometries they determined the load-displacement diagrams together with the study of the ovalization, which is the characteristic plastic deformation of the chord circumference at the brace intersection. The applied finite element model can be seen on (Figure 2.5).

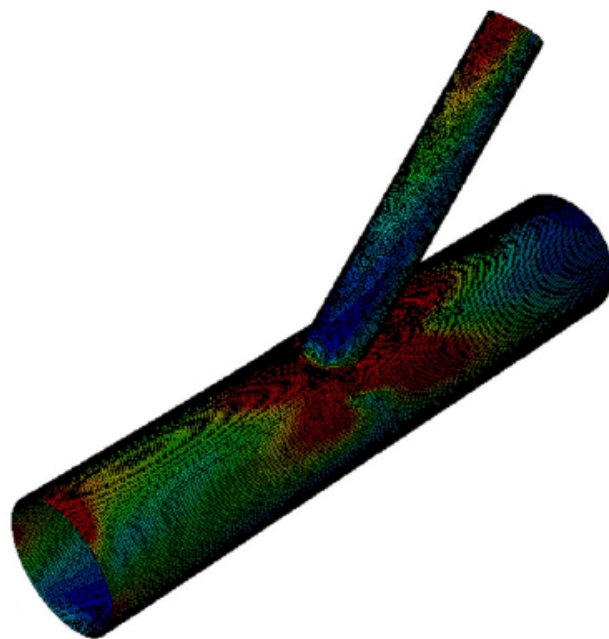


Figure 2.5. Numerical model of the investigated T and Y joints (Lesani, Bahaari, & Shokrieh, 2013)

2.4. Design methods

The current valid European standard, the Eurocode contains the necessary design formulae of hollow section joints in (Eurocode 3 EN 1993-1-8:2005 (E), 2005). At this part, a wide range of connections can be found. Before the calculation of the resistances, the EC prescribe some geometric restrictions corresponding to the hollow sections, but with this step the general six failure modes can be reduced to only two mode (*Chapter 2.2*). The design formulae are available for axial load, in plane and out of plane bending, furthermore it provides an interaction formula for the case of combined loading. It is very important that this part does not contain the necessary modifications for the case of high strength steels, it is in (Eurocode 3 EN 1993-1-12:2007:E, 2007), the further details can be found in *Chapter 3.1.2*. Beside the Eurocode, in the practice the recommendations of the CIDECT (Construction with Hollow Steel Sections) design guide is also widely used, although this is not official, only a proposition. In case of hollow section T joints, practically it offers the same formulae for the design resistances as the Eurocode.

3. Design method according to the EC3-1-8

In the Eurocode 3-1-8, Chapter 7 deals with the hollow section joints, involving many types of members (CHS, RHS, SHS, gusset plates, I girders, etc.). The purpose of this part is to give a brief review on the design aspects on these connections together with the resistance formulae, taking into account the specific limitations due to the high strength steel. Generally, if we consider the hollow section joints, we can distinguish many types, such as K, T, KT, N, X, etc. joints, but in this work, from this large set I will focus only to *T connections made of CHS members*.

3.1. Review on the design of T joints according to the Eurocode

It is worth to mention that this chapter of the standard provides design formulae to static resistance, but does deal with the fatigue problems, the high strength steels and the member resistances. The first one is not considered in this study, but if we apply HSS steels we must use the prescriptions of the EC-3-12, and in case of axially loaded members (chord or brace) the EC-3-1-1, beside the following design aspects, formulae.

3.1.1. Geometric restrictions

Before the actual design of the joints, the EC prescribes some geometric restrictions (Eurocode 3 EN 1993-1-8:2005 (E), 2005) on the shape of the members and connections, which provides the validity to the usage of the resistance formulae. Generally, these constraints are not so strict, the applicable dimensions are within a large scale. Now let us summarize the specific geometric restrictions:

[1] the nominal wall thickness of the hollow sections should be larger or equal with 2.5 mm, and in case of the chord less than 25 mm

[2] the compressed members of the joint should satisfy the requirements for Class 1 or Class 2 according to the (Eurocode 3 EN 1993-1-1:2005 (E), 2005)

[3] the diameter of the brace to the chord ratio should be between 0.2 and 1.0:

$$0,2 \leq d_1/d_0 \leq 1,0 \quad (3.1)$$

[4] the diameter to thickness ratio of the chord should be between 10 and 50:

$$10 \leq d_0/t_0 \leq 50 \quad (3.2)$$

[5] the diameter to thickness ratio of the brace should be less than 50:

$$d_1/t_1 \leq 50 \quad (3.3)$$

3.1.2. Design formulae

As it was mentioned, beside the formulae of the Eurocode 3-1-8, the design resistances of the brace and chord members should be determined according to the (Eurocode 3 EN 1993-1-1:2005 (E), 2005) for axial loading. In this work I consider only such assemblies which satisfies the geometric (in the engineering practice, usually these constraints are easy to keep) and section Class requirements, thus only the *flexural buckling failure mode* should be considered beside the following formulae in case of the compression members.

According to the applied material grade, the static design resistance should be reduced by a factor prescribed in the standard. If it is between S355 and S460, this factor is 0.9 (Eurocode 3 EN 1993-1-8:2005 (E), 2005), but if we apply HSS (greater than s460), according to (Eurocode 3 EN 1993-1-12:2007:E, 2007) this reduction factor changes to 0.8. This procedure takes into account the larger deformations in case of chord plastification (thus for the other failure modes this reduction is quite conservative). In 2004, the researchers verified the 0.9 value by laboratory tests, and recommended the 0.8 value for higher steel grades, but it is only an assumption, it has not been proved yet (Gogou, 2012).

Now, let us consider the different resistance formulae for the case of T joints, consist of Circular Hollow Section members, made of HSS. As it was mentioned in *Chapter 1.2*, only two failure modes are needed to be taken into account (if we keep the geometric prescriptions), namely the *chord face failure* and *punching shear failure*, thus only these modes are considered in this part. The notation of the joint can be seen on (*Figure 3.1*).

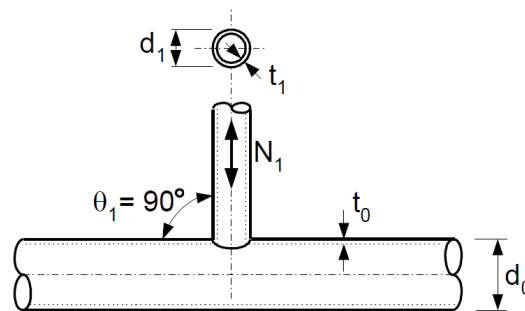


Figure 3.1 Notation of a general T joint
(Wardenier, Kurobane, Packer, Vegte, & Zhao, 2008)

Axial resistances

[1] In case of *chord face failure*, the axial resistance is:

$$N_{1,Rd} = \frac{\gamma^{0,2} k_p f_{y0} t_0^2}{\sin \theta_1} (2,8 + 14,2 \beta^2) \frac{0,8}{\gamma_{M5}}, \quad (3.4)$$

where γ is the half diameter to thickness ratio:

$$\gamma = \frac{d_0}{2t_0}, \quad (3.5)$$

f_{y0} is the yield strength of the chord material, t_0 is the thickness of the chord, 0.8 is the reduction factor correspond to the high strength steel, γ_{M5} is the partial safety factor for hollow section joints (its value is 1.0), β is the ratio of the mean diameter of the brace to the chord:

$$\beta = \frac{d_1}{d_0}, \quad (3.6)$$

and k_p is the chord stress factor:

$$k_p = \min(1 - 0,3n_p(1 + n_p), 1) \text{ for compression, and } 1 \text{ for tension,} \quad (3.7)$$

where n_p is the ratio of the maximum compressive stress in the chord to the yield strength:

$$n_p = \frac{\sigma_{0,Ed}}{f_{y0}}. \quad (3.8)$$

[2] For the case of *punching shear failure*, the axial resistance formula:

$$\text{if } d_1 \leq d_0 - 2t_0: N_{1,Rd} = \frac{f_{y0}}{\sqrt{3}} t_0 \pi d_1 \frac{1 + \sin \theta_1}{2 \sin^2 \theta_1} \frac{0,8}{\gamma_{M5}}. \quad (3.9)$$

In plane and out of plane moment resistances

In case of T connections, the two types of moment loading can be seen on (Figure 3.2).

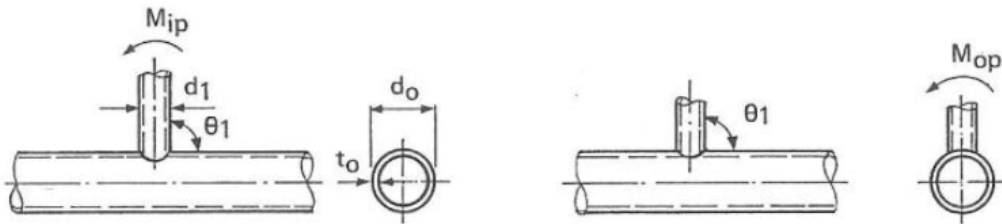


Figure 3.2. In plane and out of plane moments in case of T connections (Wardenier, Kurobane, Packer, Vegte, & Zhao, 2008)

[1] In plane moment resistance in case *chord face failure*:

$$M_{ip,1,Rd} = 4,85 \frac{f_{y0} t_0^2 d_1}{\sin \theta_1} \sqrt{\gamma} \beta k_p \frac{0,8}{\gamma_{M5}}. \quad (3.10)$$

[2] Out of plane moment resistance in case *chord face failure*:

$$M_{op,1,Rd} = \frac{f_{y0} t_0^2 d_1}{\sin \theta_1} \frac{2,7}{1 + 0,81\beta} k_p \frac{0,8}{\gamma_{M5}}. \quad (3.11)$$

[3] In plane moment resistance for the case of *punching shear failure*:

$$M_{ip,1,Rd} = \frac{f_{y0} t_0 d_1^2}{\sqrt{3}} \frac{1 + 3 \sin \theta_1}{4 \sin^2 \theta_1} \frac{0,8}{\gamma_{M5}}, \quad (3.12)$$

[4] Out of plane moment resistance for the case of *punching shear failure*

$$M_{op,1,Rd} = \frac{f_{y0} t_0 d_1^2}{\sqrt{3}} \frac{3 + \sin \theta_1}{4 \sin^2 \theta_1} \frac{0,8}{\gamma_{M5}}. \quad (3.13)$$

3.2. Design resistances of the investigated T joints according to the standard

The object of this study is to improve the design resistance formula of these T joints, but for this purpose, a wide range of hollow section dimensions should be investigated. In the practice, there are only a few manufacturer, who produce high strength steel CHS sections, from them I chose the products of the *Continental Steel Pte Ltd*. From the homepage of this company, the available dimensions can be downloaded (Cold Formed Hollow Sections, 2013). According to this brochure, I composed fourteen assemblies (*Table 3.1*), applying four different chord sizes and five different brace sizes.

	Diameter of the chord (d₀) [mm]	Thickness of the chord (t₀) [mm]	Diameter of the brace (d₁) [mm]	Thickness of the brace (t₁) [mm]
[1]	508	25	406	20
[2]	508	25	323.9	14
[3]	508	25	244.5	12
[4]	508	25	168.3	8
[5]	508	25	101.6	5
[6]	406	20	323.9	14
[7]	406	20	244.5	12
[8]	406	20	168.3	8
[9]	406	20	101.6	5
[10]	323.9	14	244.5	12
[11]	323.9	14	168.3	8
[12]	323.9	14	101.6	5
[13]	244.5	12	168.3	8
[14]	244.5	12	101.6	5

Table 3.1. *The fourteen applied assemblies (own source)*

In the numerical model, I use relatively small brace lengths, thus in this way the flexural buckling failure mode can be avoided, only the compression/bending moment resistance of the brace cross section should be calculated. In the following, I will check the geometric restrictions

and calculate the design resistances for the first assembly in detail, after that I summarize the results in tabulated form for all the others.

3.2.1. Checking of the geometric constraints for the first assembly

Initial data

$$\begin{array}{ll}
 d_0 = 508 \text{ mm} & t_0 = 25 \text{ mm} \\
 d_1 = 406 \text{ mm} & t_1 = 20 \text{ mm} \\
 f_{y0} = 690 \text{ MPa} & \gamma_{M5} = 1 \\
 \beta = \frac{d_1}{d_0} = 0,799 & \gamma = \frac{d_0}{2t_0} = 12,70 \\
 \theta_1 = 90^\circ & \gamma_{M0} = 1
 \end{array}$$

Checking of the thickness of the chord and brace

$$t_1 \geq 2 \text{ mm}, \quad t_0 \geq 2 \text{ mm} \text{ and } t_0 \leq 25 \text{ mm}, \quad (3.14)$$

where all thicknesses are within the allowable range.

Checking of the section Class

The limit of the Class 2:

$$70\epsilon^2 = 70 \frac{235}{f_{y0}} = 23,841 > \frac{d_1}{t_1} = 20,300, \quad (3.15)$$

thus, this section is Class 3.

Checking the diameter of the brace to the chord

$$0,2 \leq \frac{d_1}{d_0} = 0,799 \leq 1,0. \quad (3.16)$$

Checking the diameter to thickness ratio of the chord

$$10 \leq \frac{d_0}{t_0} = 20,320 \leq 50. \quad (3.17)$$

Checking the diameter to thickness ratio of the brace

$$\frac{d_1}{t_1} = 20,300 \leq 50. \quad (3.18)$$

3.2.2. Determine the static resistances for the first assembly

Design axial resistance

[1] Chord face failure

As we can see from equation (3.7) and (3.8), k_p is the function of the maximal compressive stress in the chord, thus the axial normal force, and in this case the design axial resistance. Practically, it means that we have to use an iterative method to calculate the resistance of the joint. Firstly, let us determine the maximal normal stress in the chord. The compression of the brace results in the bending of the chord, thus for this purpose the classical equation of the elementary strength of materials is used (of course, this is an approximation). The maximal bending moment from a concentrated load (applied at the middle of the girder), and the corresponding normal stress in the chord:

$$M_{0,Ed} = \frac{Fl}{8} = \frac{N_{1,Rd}l}{8}, \quad \sigma_{0,Ed} = \frac{M_{0,Ed}}{I_x} \frac{d_0}{2}, \quad (3.19)$$

where l is the length of the chord¹ and I_x is the secondary moment about any axis which passes through the centre of gravity:

$$I_x = \frac{\left[\left(\frac{d_0}{2} \right)^4 - \left(\frac{d_1}{2} \right)^4 \right]}{4}. \quad (3.20)$$

From this, the value of k_p and n_p can be determined:

$$n_p = \frac{N_{1,Rd}l}{8I_x} \frac{d_0}{2f_{y0}}, \quad k_p = \min \left(1 - 0,3 \frac{N_{1,Rd}l}{8I_x} \frac{d_0}{2f_{y0}} \left(1 + \frac{N_{1,Rd}l}{8I_x} \frac{d_0}{2f_{y0}} \right), 1 \right). \quad (3.21)$$

Now, if we substitute (3.21) into (3.4):

$$N_{1,Rd} = \left(1 - 0,3 \frac{N_{1,Rd}l}{8I_x} \frac{d_0}{2f_{y0}} \left(1 + \frac{N_{1,Rd}l}{8I_x} \frac{d_0}{2f_{y0}} \right) \right) \frac{\gamma^{0,2} k_p f_{y0} t_0^2}{\sin \Theta_1} (2,8 + 14,2\beta^2) \frac{0,8}{\gamma_{M5}}. \quad (3.22)$$

By this step, we get an implicit formula for the axial resistance, thus we need to apply iteration technique. I solve this problem in *MS Excel 2013*, where the last value of the k_p reduction parameter:

$$k_{p,last} = 0,9358. \quad (3.23)$$

¹ In case of compression it is $5 \cdot d_0$. The reason and determination of this size can be found in Chapter 4., and of course the same dimensions are applied in the numerical simulations.

Finally, the axial resistance, according to (3.4):

$$N_{1,Rd,cff} = \frac{\gamma^{0,2} k_p f_{y0} t_0^2}{\sin \theta_1} (2,8 + 14,2\beta^2) \frac{0,8}{\gamma_{M5}} = 6093,29 \text{ kN}. \quad (3.24)$$

[2] *Punching shear failure*

In this case, we do not need any special solution methodology, only the application of the design formula. Firstly, let us check the necessity of this failure mode:

$$d_1 = 406 \text{ mm} \leq d_0 - 2t_0 = 468 \text{ mm}, \quad (3.25)$$

thus we must take into account the *punching shear failure*:

$$N_{1,Rd,psf} = \frac{f_{y0}}{\sqrt{3}} t_0 \pi d_1 \frac{1 + \sin \theta_1}{2 \sin^2 \theta_1} \frac{0,8}{\gamma_{M5}} = 10162,35 \text{ kN}. \quad (3.26)$$

[3] *Normal resistance of the brace*

Because the flexural buckling is not considered, the compressive resistance of the brace is equal with the tensile resistance, namely:

$$N_{1,Rd,nr} = \frac{\left[\left(\frac{d_1}{2} \right)^2 - \left(\frac{d_1}{2} - t_1 \right)^2 \right] \pi}{\gamma_{M0}} f_{y0} = 16734,64 \text{ kN}. \quad (3.27)$$

The final axial resistance is smallest one from the previously determined values:

$$N_{1,Rd,Ec} = \min(N_{1,Rd,cff}; N_{1,Rd,psf}; N_{1,Rd,nr}) = 6093,29 \text{ kN}. \quad (3.28)$$

Design in plane moment resistance

[1] *Chord face failure*

Similarly to the previous case, this failure mode is also the function of the maximum normal stress in chord, so that I apply the same method to calculate the bending moment resistance. The in plane bending of the joint leads to the concentrated bending of the chord. The maximal bending moment from a concentrated moment (applied at the middle of the girder) and the corresponding normal stress in the chord:

$$M_{0,Ed} = \frac{M_{ip,1,Rd}}{4}, \quad \sigma_{0,Ed} = \frac{M_{0,Ed}}{I_x} \frac{d_0}{2}. \quad (3.29)$$

Now, the value of k_p and n_p :

$$n_p = \frac{M_{ip,1,Rd}}{4I_x} \frac{d_0}{2f_{y0}}, k_p = \min\left(1 - 0,3 \frac{M_{ip,1,Rd}}{4I_x} \frac{d_0}{2f_{y0}} \left(1 + \frac{M_{0,Ed}}{I_x} \frac{d_0}{2f_{y0}}\right), 1\right). \quad (3.30)$$

Now, if we substitute (3.23) into (3.10) the moment resistance, we get:

$$M_{ip,1,Rd} = 1 - 0,3 \frac{M_{ip,1,Rd}}{4I_x} \frac{d_0}{2f_{y0}} \left(1 + \frac{M_{ip,1,Rd}}{4I_x} \frac{d_0}{2f_{y0}}\right) 4,85 \frac{f_{y0} t_0^2 d_1}{\sin \theta_1} \sqrt{\gamma} \beta \frac{0,8}{\gamma_{M5}}. \quad (3.31)$$

The final resistance after the iteration:

$$M_{ip,1,Rd.cff} = 4,85 \frac{f_{y0} t_0^2 d_1}{\sin \theta_1} \sqrt{\gamma} \beta k_p \frac{0,8}{\gamma_{M5}} = 1730,58 \text{ kNm}. \quad (3.32)$$

[2] Punching shear failure

The moment resistance for the case of *punching shear*:

$$M_{ip,1,Rd.psf} = \frac{f_{y0} t_0 d_1^2}{\sqrt{3}} \frac{1 + 3 \sin \theta_1}{4 \sin^2 \theta_1} \frac{0,8}{\gamma_{M5}} = 1313,32 \text{ kNm}. \quad (3.33)$$

[3] Bending resistance of the brace

The plastic section modulus of the brace:

$$w_{pl} = 2 \left[\frac{\left(\frac{D_1}{2}\right)^2 \pi 4 \frac{D_1}{2}}{2 \cdot 3\pi} - \frac{\left(\frac{D_1}{2} - t\right)^2 \pi 4 \left(\frac{D_1}{2} - t\right)}{2 \cdot 3\pi} \right] = 2982,59 \text{ cm}^3, \quad (3.34)$$

thus the bending resistance:

$$M_{ip,1,Rd.br} = \frac{w_{pl} f_{y0}}{\gamma_{M0}} = 2057,98 \text{ kNm}. \quad (3.35)$$

The final resistance is the smallest of these three resistances:

$$M_{ip,1,Rd,Ec} = \min(M_{ip,1,Rd.cff}; M_{ip,1,Rd.psf}; M_{ip,1,Rd.br}) = 1313,32 \text{ kNm}. \quad (3.36)$$

Design out of plane moment resistance

[1] Chord face failure

In this case, I neglect the normal stresses coming from the warping of the chord due to the out of plane bending, and use I for the value of k_p . Thus, the out of plane moment resistance for chord face failure:

$$M_{op,1,Rd.cff} = \frac{f_{y0} t_0^2 d_1}{\sin \theta_1} \frac{2.7}{1 + 0,81\beta} k_p \frac{0,8}{\gamma_{M5}} = 586,08 \text{ kNm}. \quad (3.37)$$

[1] *Punching shear failure*

$$M_{op,1,Rd.psf} = \frac{f_{y0} t_0 d_1^2}{\sqrt{3}} \frac{3 + \sin \theta_1}{4 \sin^2 \theta_1} \frac{0,8}{\gamma_{M5}} = 1641,65 \text{ kNm}. \quad (3.38)$$

[2] *Bending resistance of the brace*

The bending resistance of the section is exactly the same as in case of in plane bending:

$$M_{op,1,Rd.br} = \frac{w_{pl} f_{y0}}{\gamma_{M0}} = 2057,98 \text{ kNm}. \quad (3.39)$$

Finally, the out of plane moment resistance:

$$M_{op,1,Rd,Ec} = \min(M_{op,1,Rd.cff}; M_{op,1,Rd.psf}; M_{op,1,Rd.br}) = 586,08 \text{ kNm}. \quad (3.40)$$

3.2.3. Tabulated results for all the assemblies

Checking of the geometric constraints

The proper geometric dimensions can be found in (Table 3.1), now only the results (Table 3.2) of the geometric checking are presented:

	$t_1 \geq 2$ mm	$t_0 \geq 2$ mm	$t_0 \leq 25$ mm	d_1/t_1	Class 2	$0,2 \leq d_1/d_0 \leq 1$	$10 \leq d_0/t_0 \leq 50$	$d_1/t_1 \leq 50$
[1]	Yes	Yes	Yes	20,30	Yes	Yes	Yes	Yes
[2]	Yes	Yes	Yes	23,14	Yes	Yes	Yes	Yes
[3]	Yes	Yes	Yes	20,38	Yes	Yes	Yes	Yes
[4]	Yes	Yes	Yes	21,04	Yes	Yes	Yes	Yes
[5]	Yes	Yes	Yes	20,32	Yes	Yes	Yes	Yes
[6]	Yes	Yes	Yes	23,14	Yes	Yes	Yes	Yes
[7]	Yes	Yes	Yes	20,38	Yes	Yes	Yes	Yes
[8]	Yes	Yes	Yes	21,04	Yes	Yes	Yes	Yes
[9]	Yes	Yes	Yes	20,32	Yes	Yes	Yes	Yes
[10]	Yes	Yes	Yes	20,38	Yes	Yes	Yes	Yes
[11]	Yes	Yes	Yes	21,04	Yes	Yes	Yes	Yes
[12]	Yes	Yes	Yes	20,32	Yes	Yes	Yes	Yes
[13]	Yes	Yes	Yes	21,04	Yes	Yes	Yes	Yes
[14]	Yes	Yes	Yes	20,32	Yes	Yes	Yes	Yes

Table 3.2. Results of the geometric checking (own source)

Axial resistances

	$N_{Rd,eff}$ [kN]	$N_{Rd,psf}$ [kN]	$N_{Rd,nr}$ [kN]	$N_{Rd,Ec}$ [kN]
[1]	6093,29	10162,36	16734,64	6093,29
[2]	4553,97	10134,20	9404,78	4553,97
[3]	3275,47	7649,93	6047,88	3275,47
[4]	2359,39	5265,78	2779,86	2359,39
[5]	1829,00	3178,86	1047,00	1047,00
[6]	3818,18	8107,36	9404,78	3818,18
[7]	2691,34	6119,94	6047,88	2691,34
[8]	1801,64	4212,62	2779,86	1801,64
[9]	1276,96	2543,09	1047,00	1047,00
[10]	1799,57	4283,96	6047,88	1799,57
[11]	1139,39	2948,84	2779,86	1139,39
[12]	729,31	1780,16	1047,00	729,31
[13]	1105,25	2527,57	2779,86	1105,25
[14]	641,16	1525,86	1047,00	641,16

Table 3.3. Axial resistances of the investigated assemblies (own source)**In plane moment resistances**

	$M_{Rd,eff}$ [kNm]	$M_{Rd,psf}$ [kNm]	$M_{Rd,mr}$ [kNm]	$M_{Rd,Ec}$ [kNm]
[1]	1730,58	1313,32	2057,98	1313,32
[2]	1101,45	835,87	928,36	835,87
[3]	627,63	476,30	447,98	447,98
[4]	297,38	225,68	141,96	141,96
[5]	108,38	82,24	32,22	32,22
[6]	881,59	668,70	928,36	668,70
[7]	502,35	381,04	447,98	381,04
[8]	238,02	180,54	141,96	141,96
[9]	86,74	65,80	32,22	32,22
[10]	329,39	266,73	447,98	266,73
[11]	156,07	126,38	141,96	126,38
[12]	56,88	46,06	32,22	32,22
[13]	142,55	108,32	141,96	108,32
[14]	51,95	39,48	32,22	32,22

Table 3.4. In plane moment resistances (own source)

Out of plane moment resistances

	$M_{Rd,eff}$ [kNm]	$M_{Rd,psf}$ [kNm]	$M_{Rd,mr}$ [kNm]	$M_{Rd,Ec}$ [kNm]
[1]	468,87	1313,32	2057,98	468,87
[2]	359,42	835,87	928,36	359,42
[3]	260,64	476,30	447,98	260,64
[4]	172,35	225,68	141,96	141,96
[5]	100,32	82,24	32,22	32,22
[6]	239,31	668,70	928,36	239,31
[7]	172,10	381,04	447,98	172,10
[8]	112,81	180,54	141,96	112,81
[9]	65,12	65,80	32,22	32,22
[10]	87,60	266,73	447,98	87,60
[11]	56,83	126,38	141,96	56,83
[12]	32,47	46,06	32,22	32,22
[13]	43,58	108,32	141,96	43,58
[14]	24,52	39,48	32,22	24,52

Table 3.5. Out of plane moment resistances (own source)

In (Table 3.3), (Table 3.4) and (Table 3.5) the most critical failure modes are highlighted, because at the numerical simulations the purpose is to determine the resistance of the connection, but in many cases the strength failure of the brace overtakes the failure of the joint. Thus, in the finite element simulations only those assemblies are considered, where the resistance of the brace is larger than the other two resistances, or the difference is less than 25 %. For example, in (Table 3.4) at the third assembly the brace failure precedes the punching failure, but they are very close to each other, the difference is about 1 %. In this case, the real failure mode cannot be predicted by the standard.

Taking into account this selecting process, in the numerical simulations the following assemblies will be considered during the different loading cases (N , M_{ip} , M_{op}):

	Diameter of the chord (d_0) [mm]	Thickness of the chord (t_0) [mm]	Diameter of the brace (d_1) [mm]	Thickness of the brace (t_1) [mm]	N	M_{ip}	M_{op}
[1]	508	25	406	20			
[2]	508	25	323,9	14			
[3]	508	25	244,5	12			
[4]	508	25	168,3	8			
[5]	508	25	101,6	5			
[6]	406	20	323,9	14			
[7]	406	20	244,5	12			
[8]	406	20	168,3	8			
[9]	406	20	101,6	5			
[10]	323,9	14	244,5	12			
[11]	323,9	14	168,3	8			
[12]	323,9	14	101,6	5			
[13]	244,5	12	168,3	8			
[14]	244,5	12	101,6	5			

Table 3.6. The selected for assemblies for the numerical simulations (own source)

4. Numerical modelling technique

The aim of this study is to investigate HSS T joints, utilizing different geometrical dimensions, and compare the numerical results with the design resistances of the standard. For this purpose, a parametric numerical model is developed in *Ansys 14.5*, where the main constituents of the model are the chord, brace and the weld region. In this chapter, firstly the development of the geometry, after that a convergence test and the validation process are discussed.

4.1. Development of the geometry

4.1.1. Joint geometry

For the creation of the geometry, instead of shell only volume elements are used, because in this way the weld region can be modelled correctly. The different constituent parts of the joint can be seen on (*Figure 4.1*).

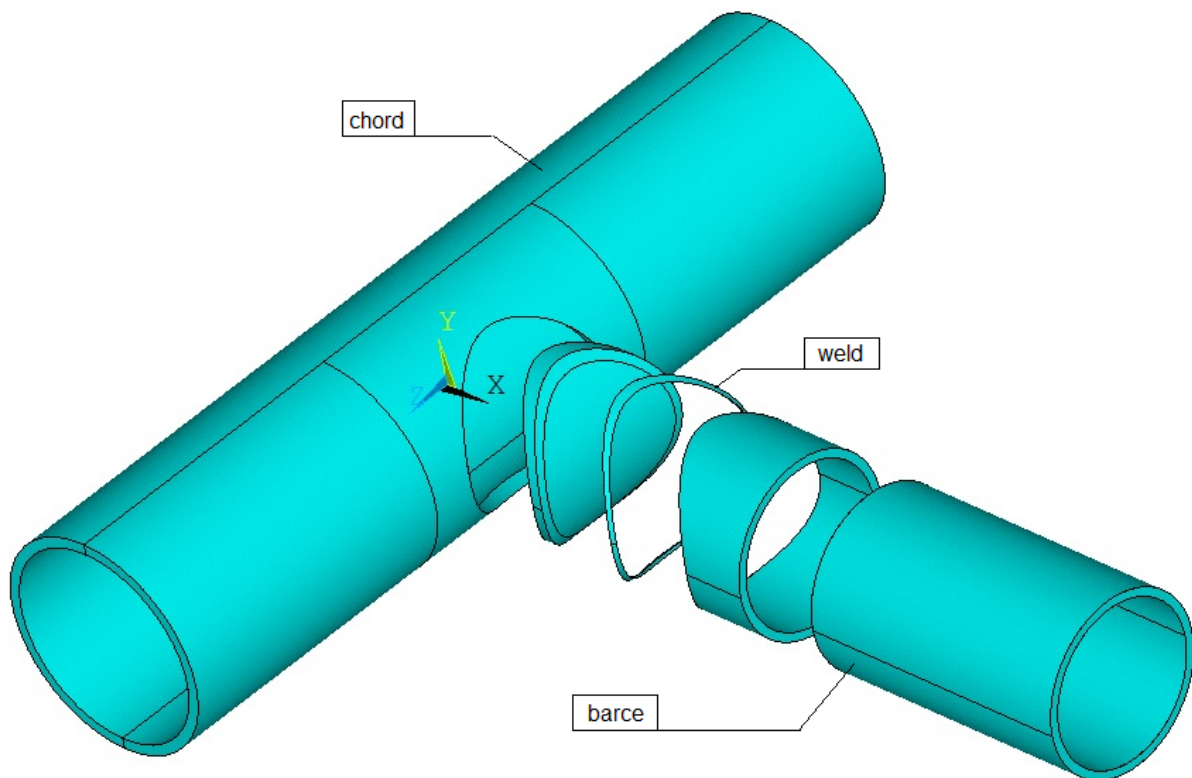


Figure 4.1. The basic constituents of the T joint (own source)

Firstly, the geometry of the chord is created, after that perpendicular brace. Those parts of the brace, which were located inside the chord are deleted, but during this process, the chord remains intact. In this figure, we can see that the volume of the chord and brace are divided into some parts, because at the inner parts of the joint (closer to the intersection line) a finer mesh will be used in order to obtain adequate results, but at the outer parts only a coarse one to reduce

the computational time. The weld region is modelled separately after the tubes, and then added to the inner volumes. The geometry of the full joint can be seen on (*Figure 4.2*).

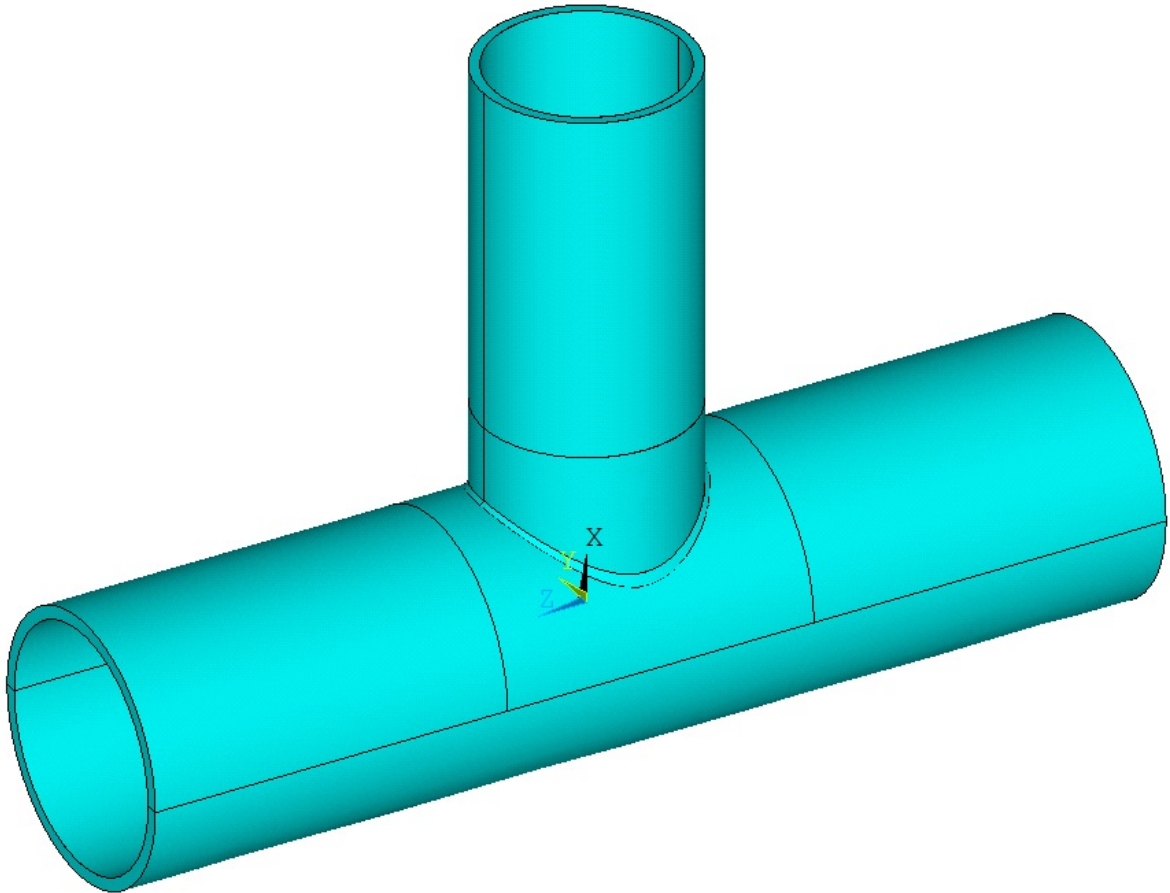


Figure 4.2. *The full geometry of the joint (own source)*

4.1.2. Modelling of the weld

Basically, in case of tubular joints two welding methods are utilized in the practice. The most widely spread type is the full penetration weld (for example in (API, 2005)), which means that the weld around the intersection of the chord and brace should be fully penetrated. Another option is when the weld starts with full penetration at the crown toe and gradually becomes a fillet weld at the crown heel. In this study, the first methodology is considered, where the weld region which locates outside of the brace is very small, thus it has no significant effect on the static strength. The effect of the weld size on the resistance is not part of this work, thus a uniform throat thickness is applied during the simulations ($a=5\text{ mm}$).

At the creation of the weld, firstly I calculate the intersection point of the weld and chord, obtaining symbolic results (in the function of throat thickness and the angle between the weld and brace). After that, the three lines which enclose the weld as a volume region are created.

Now, the areas between the lines are easy to create, and finally the volume, which is the weld region itself. The final shape of the weld can be seen on (Figure 4.3).

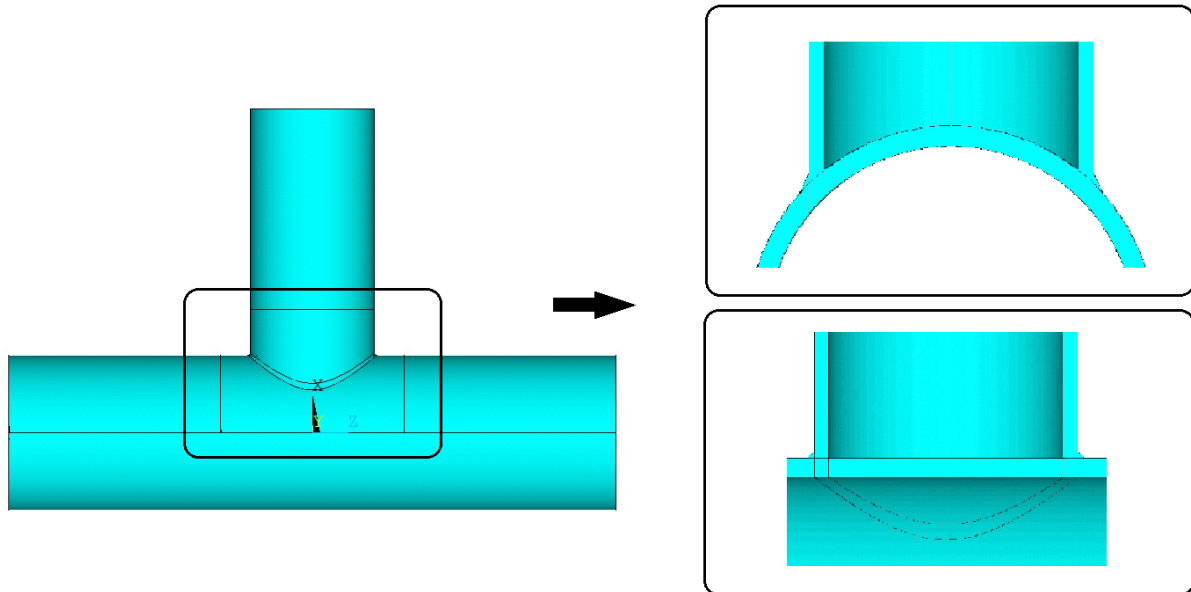


Figure 4.3. The final form of the region with two sections (own source)

4.1.3. Applied material model

In case of these steel structures the basic material models are the linear elastic, linear elastic-perfectly plastic and the linear elastic-isotropic hardening models. In this work the second model is utilized (Figure 4.4), but with a very small slope on the plastic region ($E_1/10000$) in order to promote the numerical convergence. The Young's modulus on the elastic part is 200000 N/mm^2 , and Poisson's ratio is 0,3 (Eurocode 3 EN 1993-1-1:2005 (E), 2005).

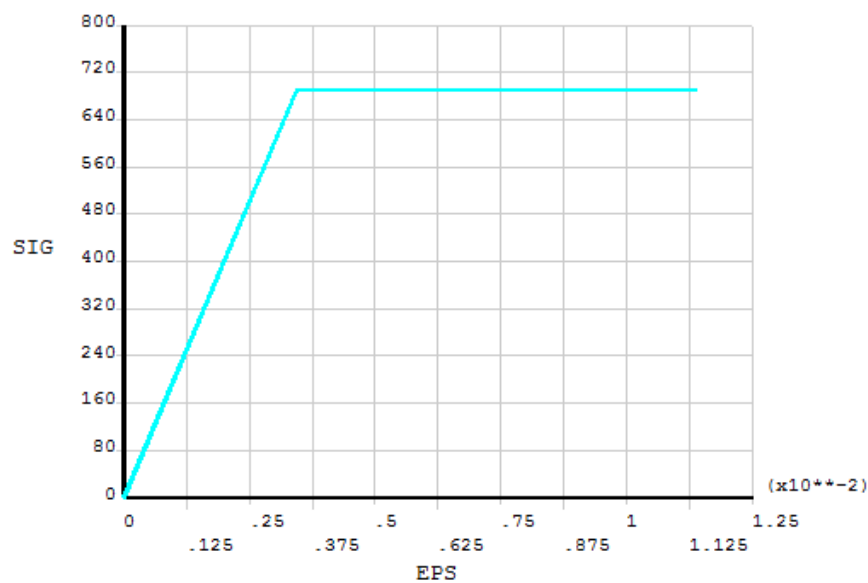


Figure 4.4. The applied material model (own source)

4.2. Convergence test, the finite element mesh generation

In this numerical model only volume elements are applied, namely SOLID187 3D 10-Node Tetrahedral Structural Solid Elements. The geometry of this finite element can be seen on (Figure 4.5).

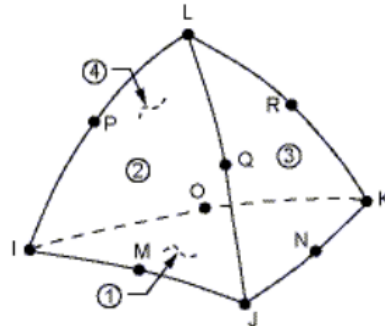


Figure 4.5. The applied SOLID187 finite element (SOLID187 Element Description, 2013)

At the territory of finite element modelling, the applied mesh size is always a critical point. To determine the adequate sizes, I perform a convergence test, which means that I utilize different mesh sizes, practically finer and finer mesh, till the mechanical response of the structure becomes repeatable. Because this model needs a very large number of elements for the correct modelling, I do not use uniform mesh size, since it would lead to an uneconomical solution (requires larger computer capacity and computational time). At this model, two different mesh sizes are applied, according to (Figure 4.6).

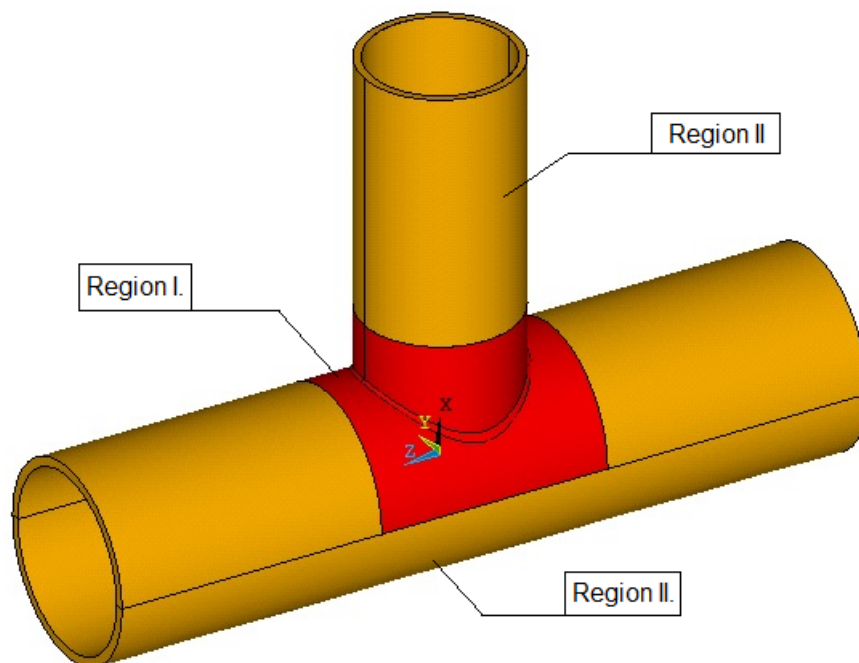


Figure 4.6. The different mesh size regions (own source)

At the middle parts of the joint, such as the weld region and some parts of the chord and brace a finer mesh is used, and the outer regions have a coarser mesh size. In the convergence test, five different mesh size sets are applied (*Table 4.1*).

First set		Second set		Third set		Fourth set		Fifth set	
I.	II.	I.	II.	I.	II.	I.	II.	I.	II.
17,5	52,5	15	45	12,5	37,5	10	30	7,5	22,5

Table 4.1. The applied mesh size sets during the convergence test (own source)

During this procedure, the brace of the T joint is subjected to compressive force, and at every timestep, the value of the force and axial displacement (parallel with the axis of the brace) are recorded. In this case, the actual values are not important, only the characteristic of the curves, which reflect the mechanical response. If the difference between the “current” and the “previous” diagrams is relatively small, the “previous” mesh size is adequate for the following numerical simulations. The force-displacement diagrams, originated from the different mesh sizes can be seen on (*Figure 4.7*).

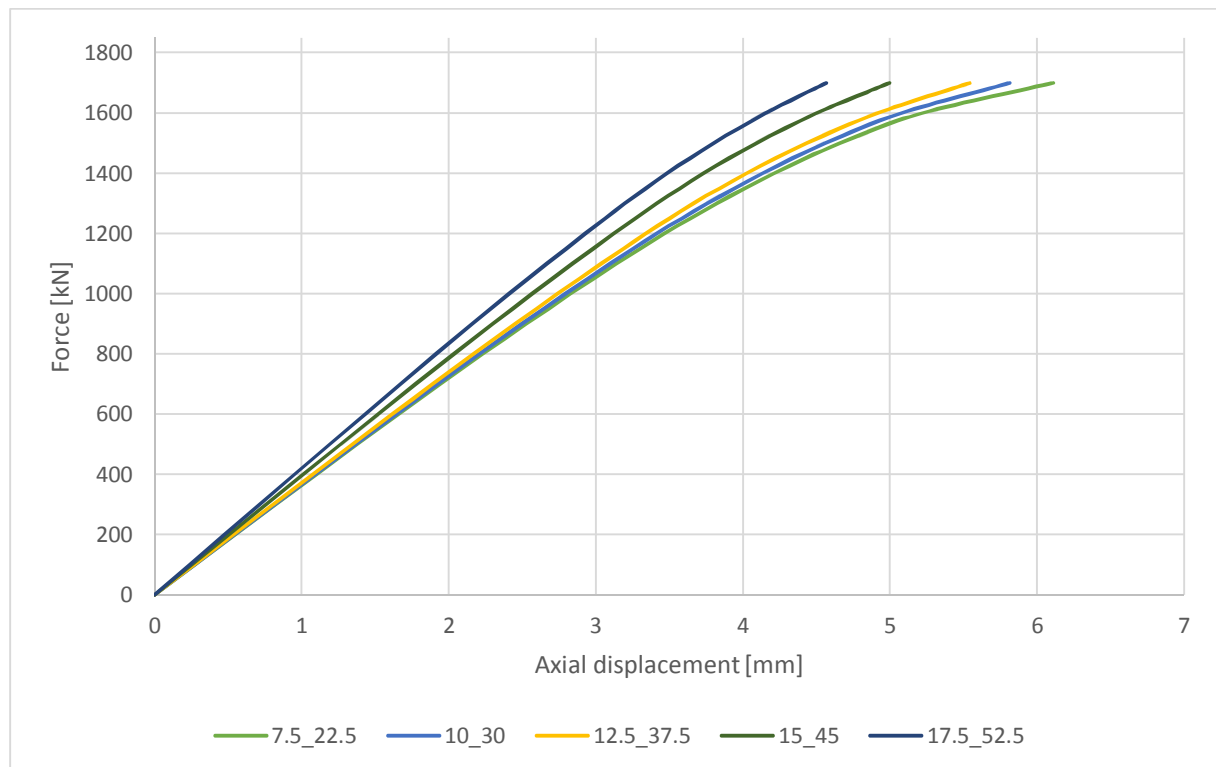


Figure 4.7. The results of the convergence, the force-displacement diagrams (own source)

From this diagram, we can see that the first and second (fourth and fifth set) curve are practically the same, thus the fourth mesh size set is used in the further calculations, namely 10 mm at the

inner parts and 30 mm at the outer regions. After this testing method, the finite element mesh can be created, (Figure 4.8) shows the result of this process, the applied mesh.

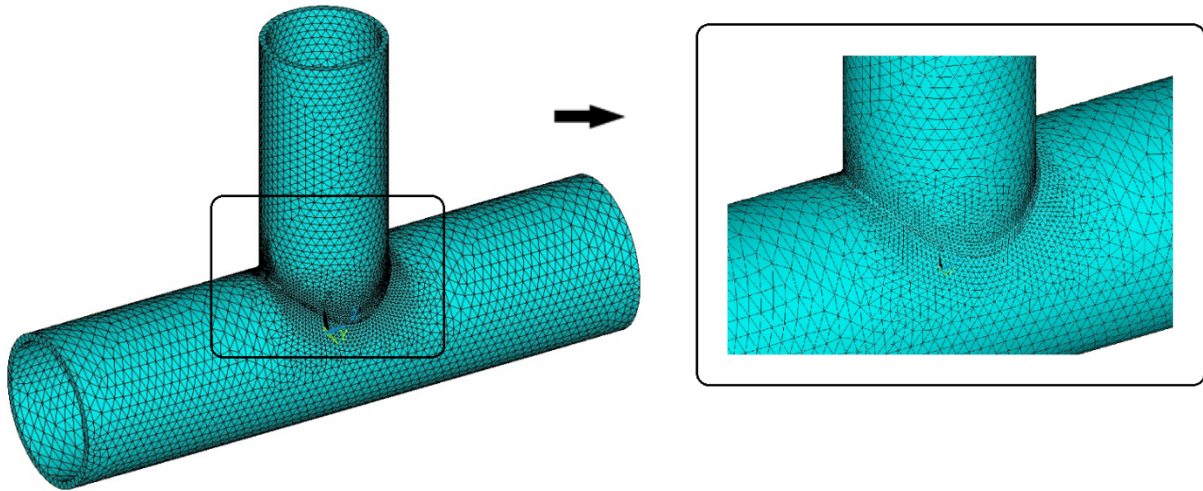


Figure 4.8. The finite element mesh of the investigated T joint (own source)

4.3. Boundary conditions

In the numerical simulations, at the ends of the chord I supported the nodes against translational motion in X, Y and Z directions, which results in a clamped support (Figure 4.9).

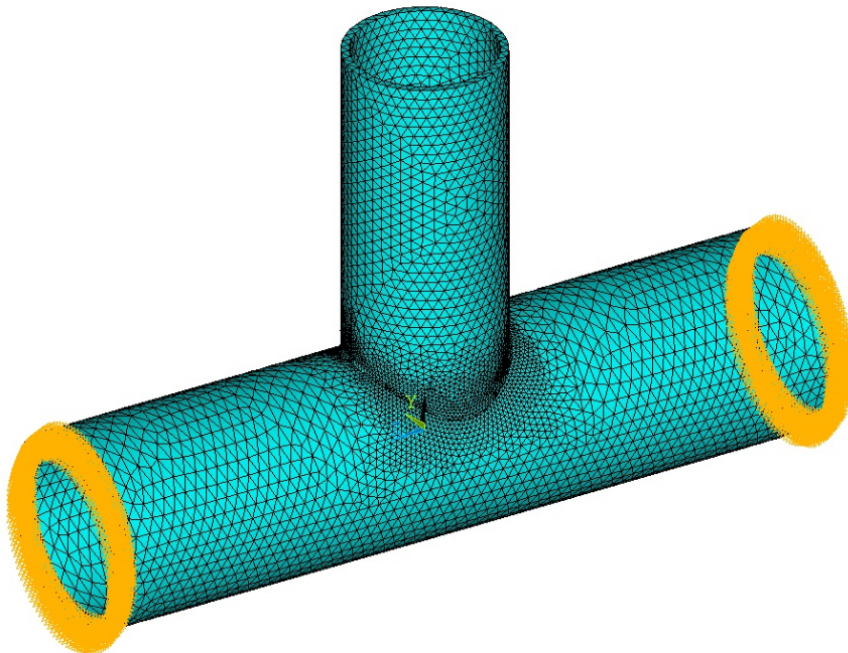


Figure 4.9. The applied clamped support at the ends of the chord (own source)

At the end of the brace, according to the applied external force system, different boundary conditions are applied. In case of compression, the end of the brace is restrained against in and out of plane translations, furthermore, in case of in plane bending the out of plane motions and in case of out of plane bending the in plane motions are inhibited. This type of support system

helps to avoid the local buckling failure of the brace, which would lead to wrong results if our aim is to determine the resistance of the joint. The applied external loads together with the boundary conditions at the end of the brace can be seen on (Figure 4.10).

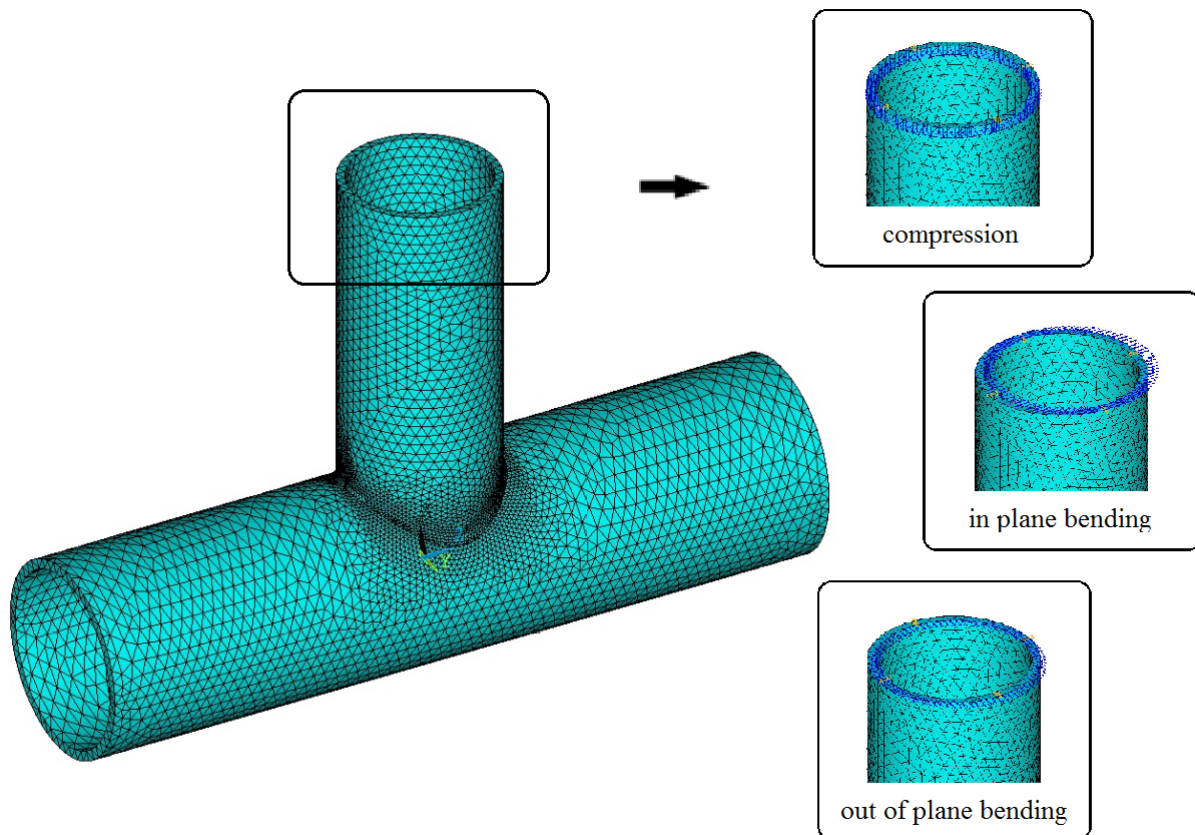


Figure 4.10. The applied boundary conditions at the end of the brace (own source)

The length of the chord has an influence on the internal forces at the intersection of the brace and chord. To obtain correct results, this phenomena should be investigated, and then minimize its effect. For this purpose, the stresses in a point, which locates on the top surface of the chord (according to (Figure 4.9)) and near to the intersection line is studied for the case of different chord lengths. The results of this parametric simulation can be seen on (Figure 4.11), where the *von Mises* stresses are illustrated in the function of chord length. Of course, the magnitude of the stresses is not relevant in this case, only the characteristic of the received curves. From this figure, we can see that in case of bending this effect tends to zero after a certain value of the length, in this study it is chosen to $9 \cdot d_0$ according to the diagram (in this test, the diameter of the chord was 500 mm, thus the 4500 mm corresponds to this size). If we consider the compression force, the stress is increasing linearly with the chord length, thus in this case the lower length is the more advantageous to reduce this effect. On the other hand, below a certain (small) size we eliminate the developing of the *chord face failure*, so taking into account these

aspects the applied length size is $5 \cdot d_0$ for the case of compression (it corresponds to the 2500 mm on the figure).

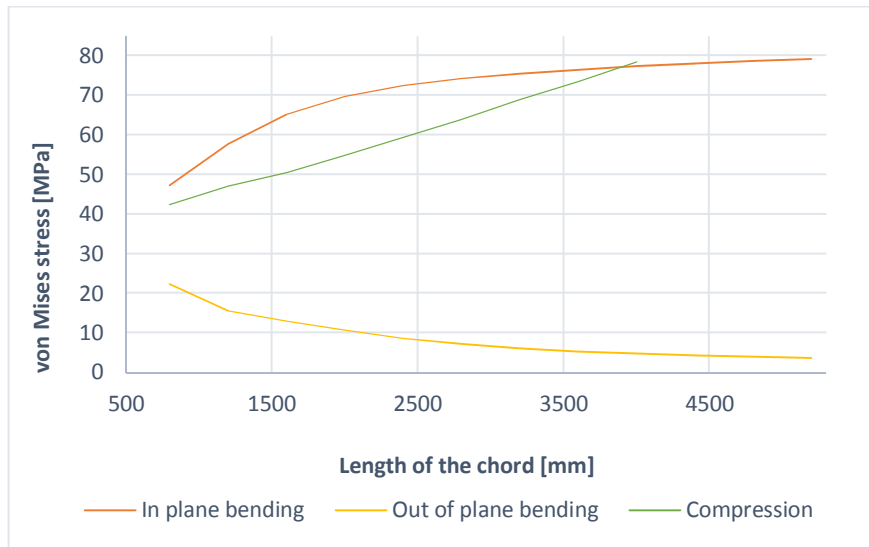


Figure 4.11. The effect of the chord length (own source)

The length of the brace should be relatively small, because in this way we can avoid the *flexural buckling* of this member. This length is set to $2 \cdot d_1$ during the numerical analyses. The applied dimensions can be seen on (Figure 4.12).

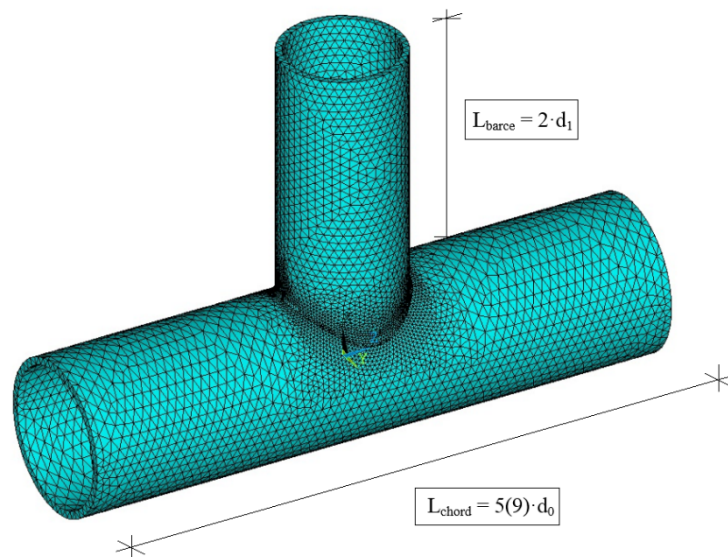


Figure 4.12. The length of the chord and brace in case of compression (bending) (own source)

4.4. Validation of the finite element model

The validation of the finite element model is based on (Lesani, Bahaari, & Shokrieh, 2013), where the results of earlier experiments are utilized. A very large number of tests were performed between 1964 and 1991 on tubular joints, and stored in database. In this case beside

the experimental, the numerical results of the article are also available. The investigated specimen was subjected to compressive force during the experiment, and had hinged supports at the ends of the chord. The proper geometric dimensions and the yield strength are listed in (Table 4.2), where the original numbering of the joints is applied.

Joint I.D.	d_0 [mm]	t_0 [mm]	d_1 [mm]	t_1 [mm]	L_{chord} [mm]	F_y [Mpa]
J10	457,6	4,9	165,2	4,7	2286	392

Table 4.2. The main geometric sizes and material properties of the specimen (Lesani, Bahaari, & Shokrieh, 2013)

The length of the brace is the half of the chord, and during the experimental and numerical tests the in and out of plane translations of the brace end were restrained, such as in this study. I applied the same material model as in the article, namely linearly elastic-perfectly plastic with 200000 N/mm^2 Young's modulus and 0,3 Poisson's ratio. At the end of the chord, in this simulation instead of the fixed support a hinged one is used (as in the experiments). Because I use volume elements, which only have translational degree of freedoms, I supported only a few nodes to allow the rotation of the model. The exact finite element model together with the boundary conditions, which are used during the validation process can be seen on (Figure 4.13).

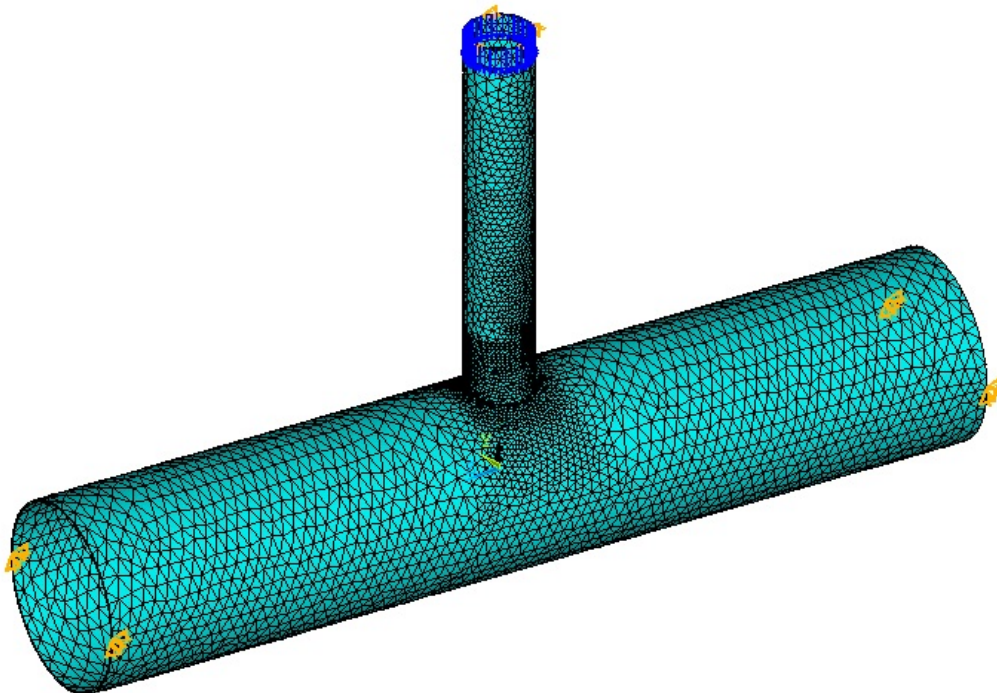


Figure 4.13. The applied finite element model for the validation (own source)

As a result of the laboratory experiments, the load bearing capacity is available, thus this value is the base of the validation. In the finite element software, the *arc-length method* is used to calculate the capacity for the nonlinear analysis. The failure criteria is based on the force-

displacement diagram, namely the load-bearing capacity is defined as the peak load on the diagram, after this value the curve starts to decrease, and that is why this method is utilized, because it is able to determine this region. The result of the simulation can be seen on (Figure 4.14), where the displacement values correspond to the end of the brace.

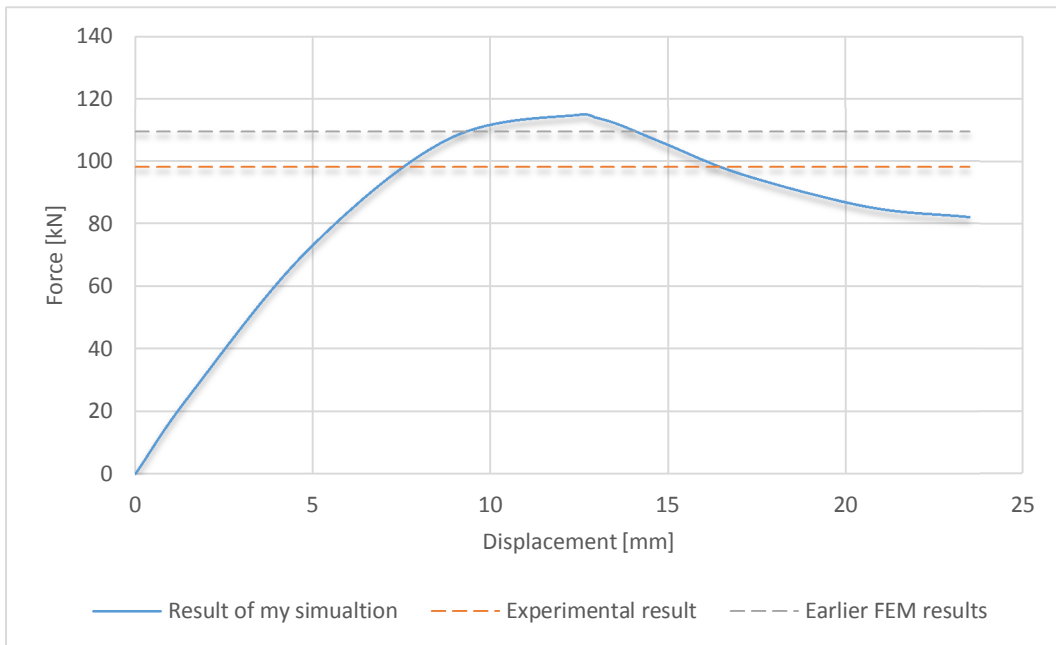


Figure 4.14. The force-displacement diagram of the validation (own source)

Now let us compare the load-bearing capacities coming from the different sources (Table 4.3). We can see that the difference between the experimental and my numerical result is about 14 %, but the exact material properties were not recorded during the experiments. Consequently, the assumed values of the validated finite element model were used in my simulation, which resulted in a very low (about 4 %) deviation between the numerical models, thus this model has been *successfully validated*.

Joint I.D.	Test result [kN]	Result of M. Lesani et al. [kN]	FEM result [kN]
J10	98,1	109,28	114,83

Table 4.3. Comparing the results of the validation process (own source)

5. Development of design formulation

The aim of this chapter is to propose a modified design formula for the joint resistance, taking into account the different loading conditions. For this purpose, firstly I perform numerous parametric simulations for compression, in plane and out of plane bending utilizing the selected assemblies (*Table 3.6*), after that I evaluate the results and determine the modified resistance formulae.

5.1. Parametric simulations

5.1.1. Analysis methodology

Similarly to the validation process, the *arc-length method* is used for the nonlinear analysis. In this study, the material and geometrical nonlinearities are considered. To reduce the computational time, the solver is terminated after the first limit point is reached, thus the force applied before the termination will be the load-bearing capacity.

5.1.2. Results for the first assembly

For the first assembly, I show the results in details, after that I summarize them in tabulated form. In case of compression, the characteristic of the failure process is the force-displacement diagram, which can be seen on (*Figure 5.1*), where the received curve reflects very well the linearly-elastic behaviour in case of lower loads, and after that the development of the plastic mechanisms. The investigated point here also the end of the brace. The load-bearing capacity is $8706,1 \text{ kN}$, which is about 42 % higher comparing to the EC resistance.

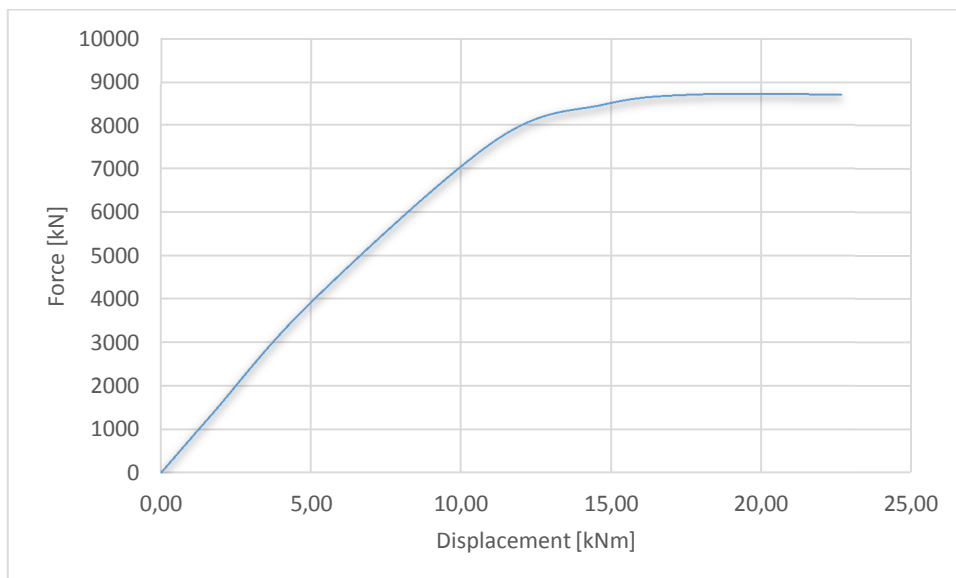


Figure 5.1. The load-displacement curve for the first assembly (own source)

The deformation and plastic strains can be seen on (Figure 5.2), where the left figure (deformation) shows properly the plastification of the chord (*chord face failure*), but at the failure only the close region around the intersection line is in plastic state.

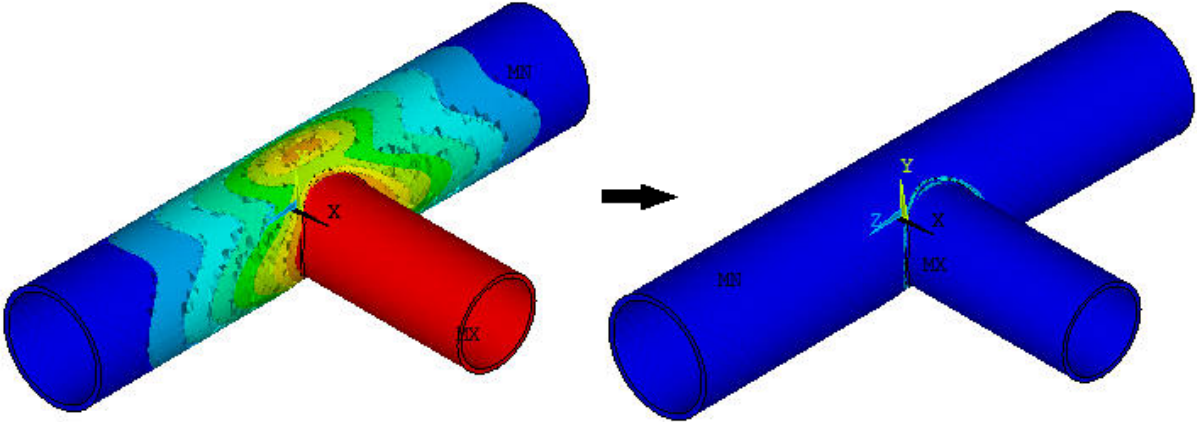


Figure 5.2. The deformation (left) and plastic strain (right) figures for compression (own source)

In case of bending, instead of the force-displacement diagram I represent the moment-rotation curves (Figure 5.3). In both cases (in and out of plane bending), the rotation is based on the displacement of the middle line of the brace, which is calculated from the average of two point locate on the diameter of the brace (we get these points at the end cross section of the brace if we intersect it with the axis of the moment vector).

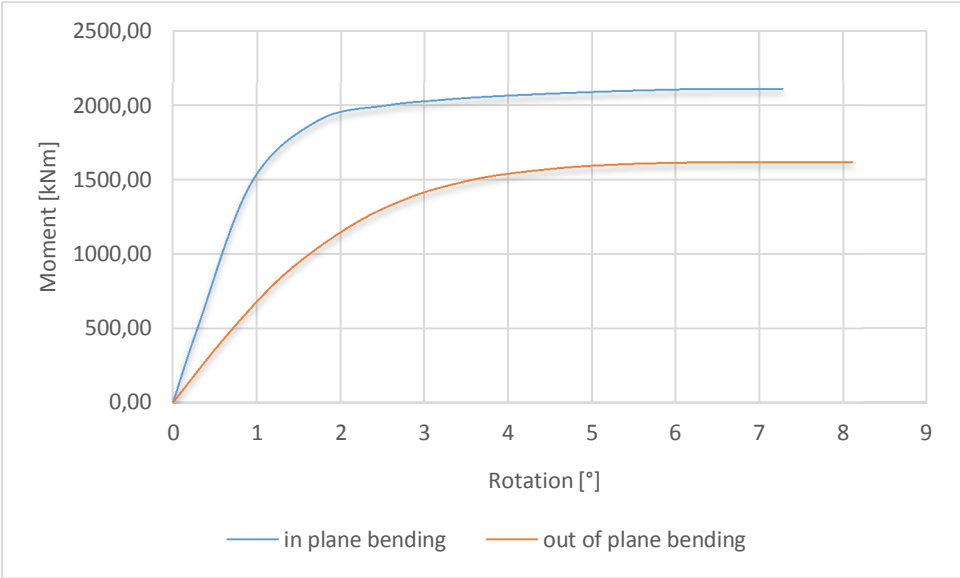


Figure 5.3. Moment-rotation curves for the first assembly (own source)

In case of these figures, we can recognize the characteristic linear-elastic-perfectly plastic behaviour again, and of course for out of plane bending the resistance is lower, in this case about with 25 %. The in plane moment resistance is 2114,31 kNm (about 61 % higher than EC

resistance), and out of plane moment resistance is $1620,22 \text{ kNm}$, which is about 245 % higher comparing to the standard resistance (the necessary conclusion is at the end of the *Chapter 5.1.2*). The deformation and plastic strains of the first assembly can be seen on (*Figure 5.4*) and (*Figure 5.5*).

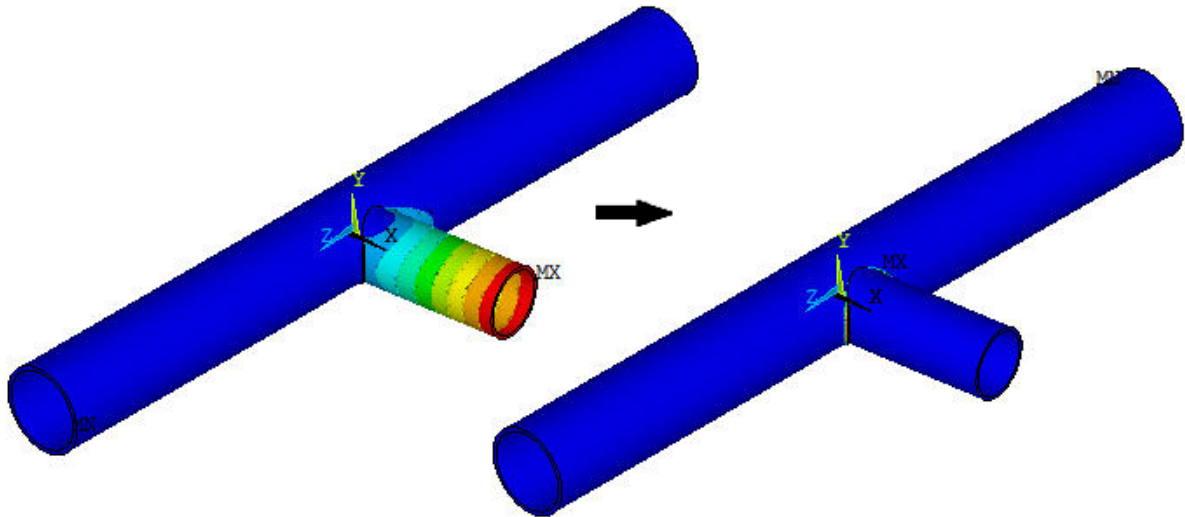


Figure 5.4. The deformation (left) and plastic strain (right) figures for in plane bending
(own source)

In case of the first figure, the *punching shear failure* mode appears, as the Eurocode predicted by the resistance formulas, but in case of the out of plane bending we can also recognize the *punching shear failure*, in contract to the EC *chord face failure* prediction. The resistance according to the Ansys also much closer to the this resistance, which means that either the chord face failure formula is too conservative, or the model is wrong, although in case of the compression and in plane bending it reflects well the failure modes, thus this problem needs further investigation.

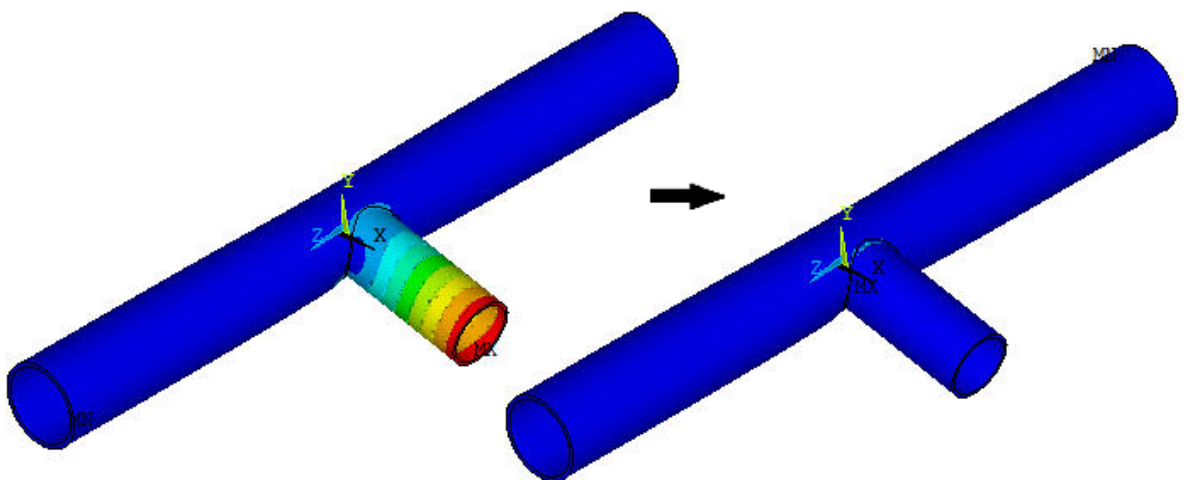


Figure 5.5. The deformation (left) and plastic strain (right) figures for out of plane bending
(own source)

5.1.3. Tabulated results for all the assemblies

For the selected assemblies I summarized the results in (Table 5.1), (Table 5.2) and (Table 5.3) together with over-capacity, according to the simulations.

Axial resistances

	$N_{Rd,Ec}$ [kN]	$N_{R,FEM}$ [kN]	$N_{Rd,Ec}/N_{R,FEM}$ [-]
[1]	6093,29	8706,10	1,43
[2]	4553,97	6359,78	1,40
[3]	3275,47	4591,88	1,40
[4]	2359,39	2630,80	1,12
[5]		-	
[6]	3818,18	5622,79	1,47
[7]	2691,34	3815,41	1,42
[8]	1801,64	2558,63	1,42
[9]		-	
[10]	1799,57	2694,64	1,50
[11]	1139,39	1667,97	1,46
[12]	729,31	1034,28	1,42
[13]	1105,25	1679,43	1,52
[14]	641,16	962,51	1,50

Table 5.1. Results of the parametric simulations for compression (own source)

In plane moment resistances

	$M_{Rd,Ec}$ [kNm]	$M_{R,FEM}$ [kNm]	$M_{Rd,Ec}/M_{R,FEM}$ [-]
[1]	1313,32	2114,31	1,61
[2]	835,87	1322,98	1,58
[3]	447,98	735,98	1,64
[4]		-	
[5]		-	
[6]	668,70	1091,35	1,63
[7]	381,04	635,03	1,67
[8]		-	
[9]		-	
[10]	266,73	431,42	1,62
[11]	126,38	214,21	1,70
[12]		-	
[13]	108,32	186,92	1,73
[14]	32,22	58,77	1,82

Table 5.2. Results of the parametric simulations for in plane bending (own source)

Out of plane moment resistances

	$M_{Rd,Ec}$ [kNm]	$M_{R,FEM}$ [kNm]	$N_{Rd,Ec}/N_{R,FEM}$ [-]
[1]	468,87	1620,22	3,46
[2]	359,42	1028,91	2,86
[3]	260,64	654,21	2,51
[4]		-	
[5]		-	
[6]	239,31	827,93	3,46
[7]	172,10	554,50	3,22
[8]	112,81	247,08	2,19
[9]		-	
[10]	87,60	550,83	6,29
[11]	56,83	204,64	3,60
[12]	32,22	65,42	2,03
[13]	43,58	166,12	3,81
[14]	24,52	57,79	2,36

Table 5.3. Results of the parametric simulations for out of plane bending (own source)

First of all, in case of compression the over-capacity of the fourth assembly is very small comparing to the other ones, thus this one needs more analysis. From the plastic strain figure (Figure 5.6), we can recognize the *failure* of the brace, thus this result should not be used for the further investigations.

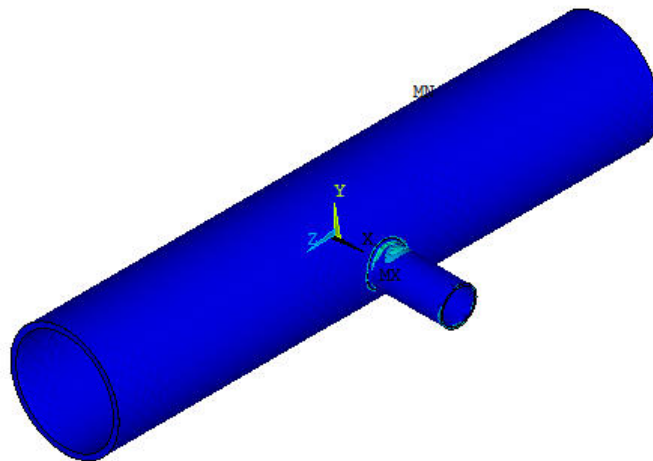


Figure 5.6. Plastic deformations of the fourth assembly (own source)

Furthermore, in case of out of plane bending, the deviations between the numerical and standard results are very large (in all cases the over-capacity is higher than 100 %), thus this loading case is not considered at the modification of the design formulae.

5.2. Modification of the design formulae

As it was mentioned in the previous chapter, only the axial and in plane bending is considered here. At the modifications, firstly I analyse the standard design formulae, then propose some modifications in that, and finally determine the introduced parameters with an optimization process, taking into account my numerical results.

5.2.1. Axial resistance

In case of compression, for all the assemblies the *chord face failure* is the critical, thus only this resistance formula can be modified according to the finite element results. The original standard formula, without the partial safety factor and reduction factor:

$$N_{Rd} = \frac{\gamma^{0,2} k_p f_{y0} t_0^2}{\sin \theta_1} \left(2,8 + 14,2 \left(\frac{d_1}{d_0} \right)^2 \right). \quad (5.1)$$

The common in this formula, and the formulae for X, K and N joints is the following term:

$$\frac{k_p f_{y0} t_0^2}{\sin \theta_1}, \quad (5.2)$$

thus in the modified formula I keep this term in this form. If we take a look at the actual failure mode (according to the experiments, for example on (Figure 2.1), it comes off around the weld, not around the brace, as the design formula implies. In this study a weld with $a=5 \text{ mm}$ was applied during the numerical simulations, which angle (α) to the brace is 30° , so its length parallel with the chord (Figure 5.8):

$$a_c = \frac{a}{\cos(\alpha)}. \quad (5.3)$$

Besides taking into account this modified size I introduce some parameters in the original formula in the following way:

$$N_{Rd,mod} = \gamma^{x_1} \left(\frac{k_p f_{y0} t_0^2}{\sin \theta_1} \right) \left(x_2 + x_3 \left(\frac{d_1 + 2a_c}{d_0} \right)^{x_4} \right). \quad (5.4)$$

Practically, this is an optimization problem, where the optimal value of the x_1 , x_2 , x_3 and x_4 parameters should be determined, taking into account the numerical results:

$$f(x_1, x_2, x_3, x_4) = N_{Rd,mod}(x_1, x_2, x_3, x_4) - N_{Rd,FEM} = \min!. \quad (5.5)$$

In this formula, f is the function to be minimized, $N_{Rd,mod}$ is the modified axial resistance function and $N_{Rd,FEM}$ represents the results obtained by the numerical simulations. There are

different ways to solve this problem, now the *nonlinear least squares method* is applied in the *Matlab R2013a mathematical software*. The received parameters are shown in (Table 5.4).

X ₁	X ₂	X ₃	X ₄
0,0999	4,8827	20,0093	2,4558

Table 5.4. The received parameters to the modified axial resistance formula (own source)

Thus, the proposed modified formula for axial compression:

$$N_{Rd,mod} = \gamma^{0,0999} \left(\frac{k_p f_{y0} t_0^2}{\sin \theta_1} \right) \left(4,8827 + 20,0093 \left(\frac{d_1 + 2a_c}{d_0} \right)^{2,4558} \right). \quad (5.6)$$

After this, the *coefficient of determination* (Cod) are calculated so that to characterize the exactness of the approximation functions. The general formula of this index-number:

$$R^2 = 1 - \frac{\sum (y - \hat{y})^2}{\sum (y - \bar{y})^2}. \quad (5.7)$$

In this equation, y refers to the measured data, \hat{y} is the fitted data and \bar{y} is the mean of the observed data. This R^2 *index-number* is always between zero and one, and the closer to the one this number the more exact the regression. Now, the received resistances (from the EC, Ansys and the modified formula) and Cod value are summarized in (Table 5.5).

	N _{Rd,Ec} [kN]	N _{R,FEM} [kN]	N _{r,mod} [kN]	CoD
[1]	6093,29	8706,10	8773,65	
[2]	4553,97	6359,78	6372,49	
[3]	3275,47	4591,88	4586,10	
[6]	3818,18	5622,79	5564,10	
[7]	2691,34	3815,41	3802,85	
[8]	1801,64	2558,63	2587,21	0,9996
[10]	1799,57	2694,64	2605,11	
[11]	1139,39	1667,97	1613,20	
[12]	729,31	1034,28	1087,02	
[13]	1105,25	1679,43	1642,98	
[14]	641,16	962,51	955,44	

Table 5.5. The standard, Ansys and modified axial resistances (own source)

For the graphical representation of the received results a column diagram is utilized (Figure 5.7), where the Ansys resistances have unit values, and the others are compared to this one:

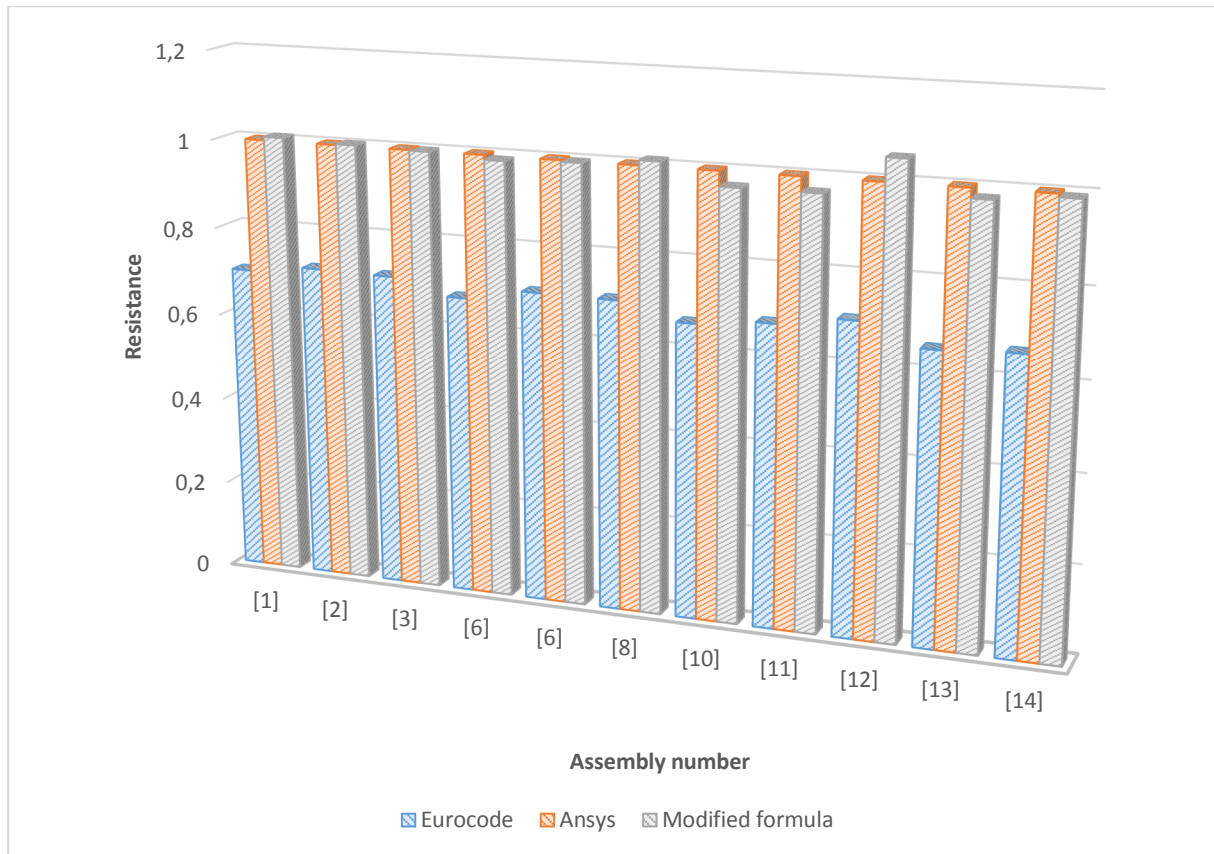


Figure 5.7. The received axial resistances, comparing to the numerical results (own source)

5.2.2. In plane bending resistance

In this case, contract to the compression the *punching shear failure* is the dominant. Utilizing the previously applied procedure, firstly let us consider the general formula for this failure (without the partial safety factor):

$$M_{ip,Rd} = \frac{f_{y0} t_0 d_1^2}{\sqrt{3}} \frac{1 + 3 \sin \theta_1}{4 \sin^2 \theta_1} 0,8 = \frac{f_{y0} t_0 d_1^2}{\sqrt{3}} 0,8 \text{ (for } T \text{ joints)}. \quad (5.8)$$

This formula does not contain experimentally determined parameters, thus we cannot apply the previous train of thought, namely the introduced parameters. In this case, the increased size of the brace by the a_c is utilized, because the actual failure occurs around the weld again, as (Figure 5.8) shows. Furthermore, the reduction factor refers to the *chord face failure*, thus we can obtain such results which are closer to the reality if we neglect it.

On these basis, the proposed modified formula:

$$M_{ip,Rd.mod} = \frac{f_{y0} t_0 (d_1 + 2a_c)^2}{\sqrt{3}}. \quad (5.9)$$

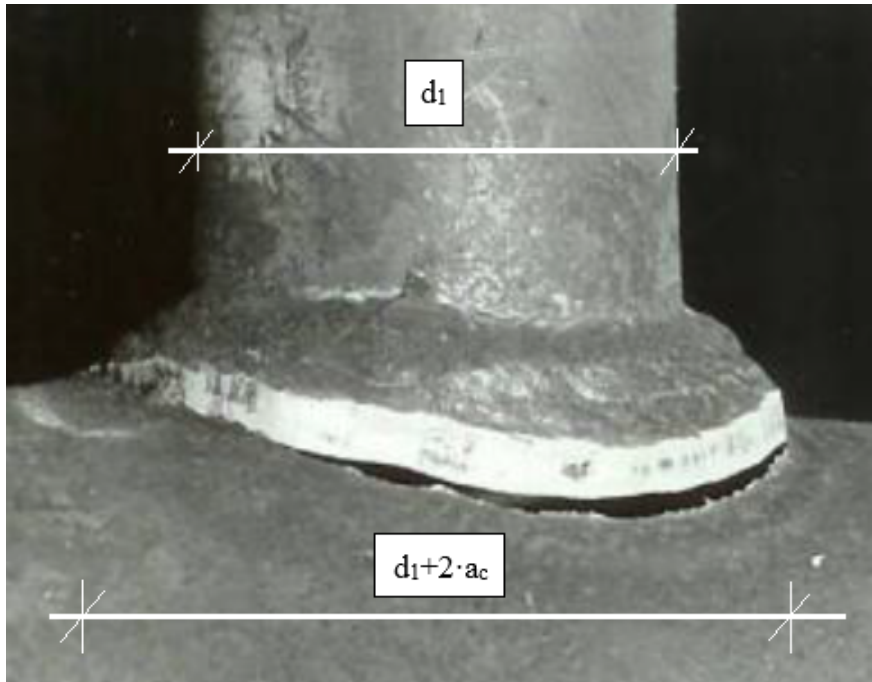


Figure 5.8. The shape of the actual failure in case of punching shear (Wardenier, Kurobane, Packer, Vegte, & Zhao, 2008)

The received moment resistances together with standard and numerical results (Table 5.6):

	$M_{Rd,Ec}$ [kNm]	$M_{R,FEM}$ [kNm]	$M_{R,mod}$ [kNm]
[1]	1313,32	2114,31	1736,36
[2]	835,87	1322,98	1120,67
[3]	447,98	735,98	652,93
[6]	668,70	1091,35	896,53
[7]	381,04	635,03	522,35
[10]	266,73	431,42	365,64
[11]	126,38	214,21	180,39
[13]	108,32	186,92	154,62
[14]	32,22	58,77	61,20

Table 5.6. The standard, Ansys and modified in plane moment resistances (own source)

Now, the resistances are still below the numerical results (except the last assembly, where the difference is very small), but significantly closer to them, which results more economical design according to the utilized material quantity. Of course, this modification is also seems to a good choice in case of the *punching shear failure* formula corresponding to compression, but in this study I cannot support this theory with numerical results (since in all cases the failure mode was chord face failure for compression)

The graphical representation of the received results from the three sources (*Figure 5.9*):

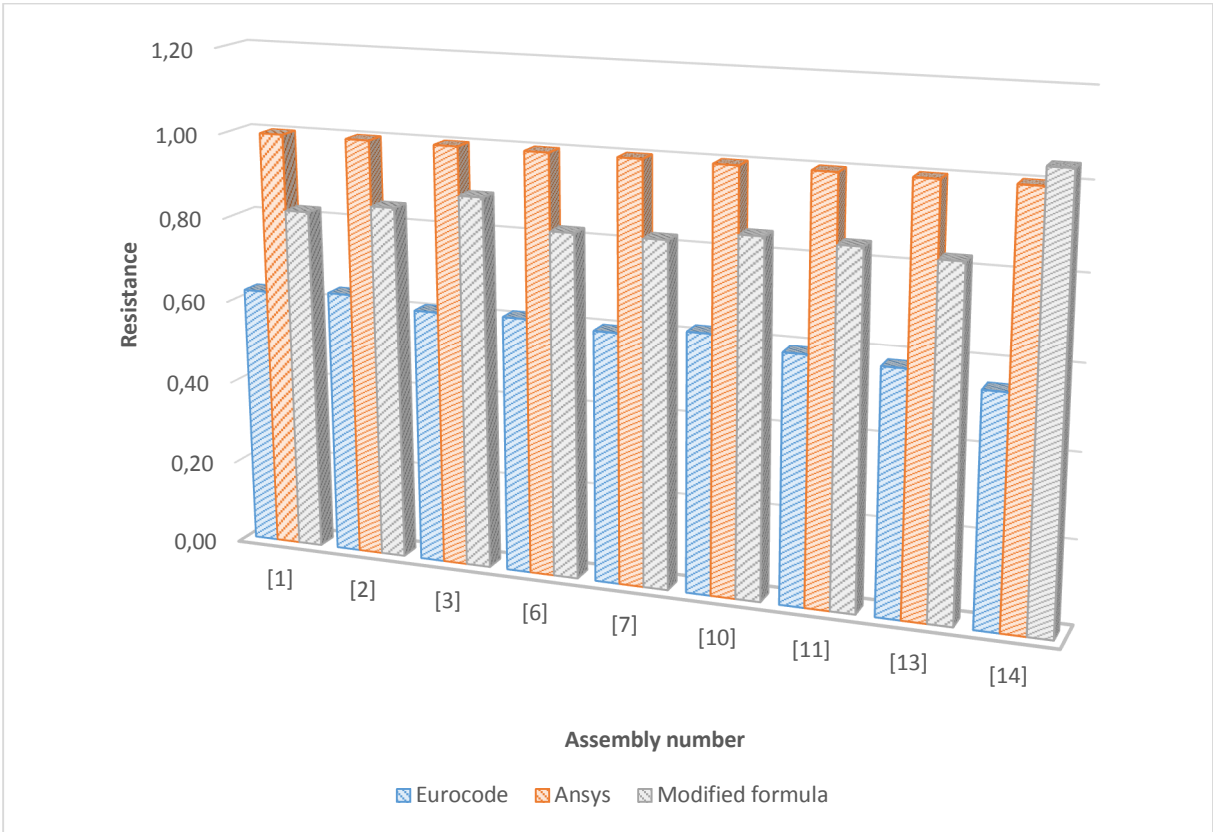


Figure 5.9 The received in plane bending resistances, comparing to the numerical results (own source)

6. Design method calibration

In this chapter, the aim is to allocate a *safety factor* for the previously determined *axial design formula*, based on stochastic analysis. For this purpose, I determine the number of necessary repetition number for the Monte-Carlo analysis, and perform the simulation in *Matlab* and *Ansys*. If the results show sufficiently correspondence, I repeat the simulation for all the assemblies in *Matlab*, and determine the final value of the partial factor.

6.1. Stochastic modelling

During these simulations, both geometric and material uncertainties are taken into account, where the exact *mean values*, *standard deviations* and *distribution types* are taken from (JCCS, 2000). At the material uncertainties the yield strength of the S690 HSS, and at the geometric uncertainties the thickness of the chord is set to stochastic variable, since it has the largest effect on the load-bearing capacity due to its quadratic form. In the *Ansys* simulations I use the *twelfth assembly*, because its running time is quite low (about four minutes) comparing to the first few assemblies, where the geometry is significantly larger, thus the necessary computational time also very high (about two hours). Unfortunately, the advised stochastic material properties are not valid for high strength steels, practically there are no available laboratory experiments on them. In this study, the necessary sources are missing to perform such tests, thus the recommendations correspond to the reinforcing steel bars are utilized. The proposed (*Table 6.1*) distributions for the chord thickness and yield strength:

	Mean value	Standard deviation	Distribution
t_0	14 mm	1 mm	Gauss
f_{y0}	750 MPa	30 MPa	Gauss

Table 6.1. *The applied stochastic variables (own source)*

In case of the chord thickness, at the calculation of the mean value the (JCCS, 2000) allows the increasing or decreasing of the characteristic value with 1 mm, but in this case there is no specific reason to change it, thus I apply the characteristic one.

6.2. Determination of the necessary repetition number

This number is always a sensitive point in the Monte-Carlo analysis, thus we have to determine it very circumspectly. The main object is to test the modified resistance formula, and determine a safety factor for that. In the *Ansys* it would take a lot of time to investigate all the assemblies in stochastic way, thus I would like to perform the necessary simulations in *Matlab*, where this time reduces to a few minutes instead of numerous days. For this purpose, firstly

with the help of the *Matlab* I determine a characteristic curve for the standard deviation of the normal resistance (all simulations in *Chapter 6.2* refers to the twelfth assembly). At this curve, I consider several repetition numbers, and for these numbers I repeat the Monte-Carlo simulation 100 000 times (in this case there were not differences in the output if I repeated this test again), and record the standard deviation of the axial resistance for each repetition number (this is very similar to the convergence test applied at the determination of the necessary mesh size). The results of these tests can be seen on (*Figure 6.1*). Practically this curve represents that if we apply a repetition number, than how much can we rely on the obtained results.

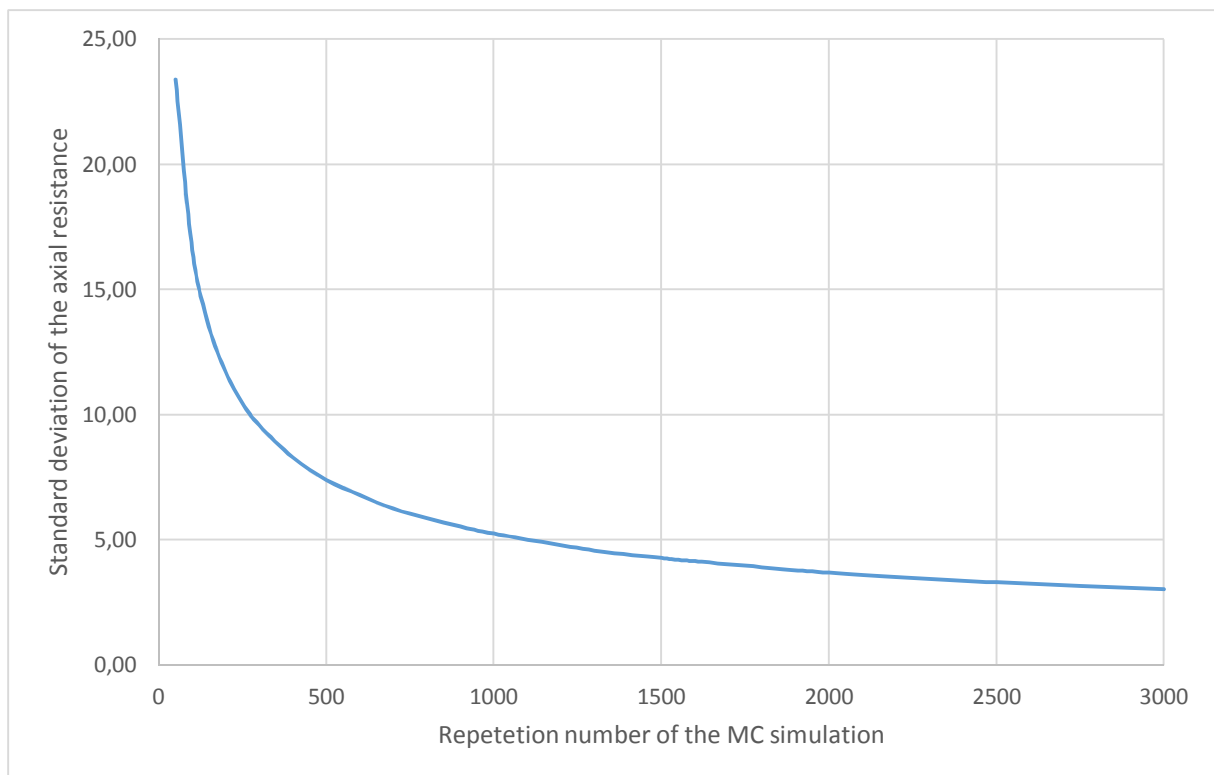


Figure 6.1. Variation of the standard deviation in the function of the repetition number
(own source)

The aim of this curve is to select such a number, which provide sufficiently reliable results. From this figure, we can see that in case of low values the connection is exponential, but after a certain value it becomes approximately linear. For the *Ansys* simulation, I chose 500, because after this value the slope of the curve significantly decreases. The purpose of the probabilistic finite element simulation is to validate my *Matlab* algorithm. Fortunately, probabilistic design is available in *Ansys*, thus after the proper definition of the stochastic variables I perform the Monte-Carlo analysis, utilizing the *Latin Hypercube Sampling* technique (LHS) (in this case, the program check the stochastically generated values before each simulation, and generates a new one if it is very close to a previously generated value, because in that case practically it

will not provide new results). The results of the MC simulation in Ansys are represented on the following figures, where the histogram of the chord thickness (*Figure 6.2*), the yield strength (*Figure 6.3*) and the axial resistance (*Figure 6.4*) can be seen (similarly to the previous Chapter, the load-bearing capacity is based on the arc-length method).

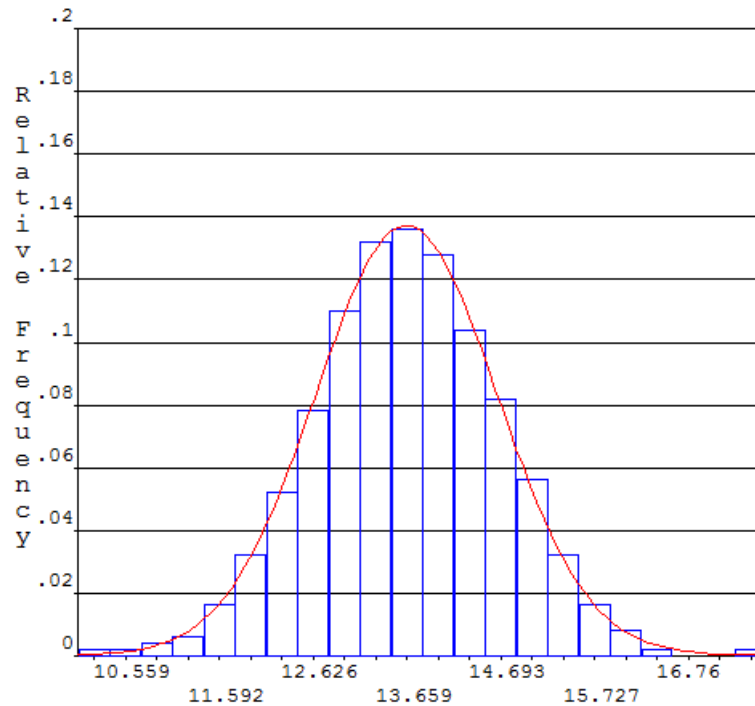


Figure 6.2. The histogram of the chord thickness obtained by the Ansys (own source)

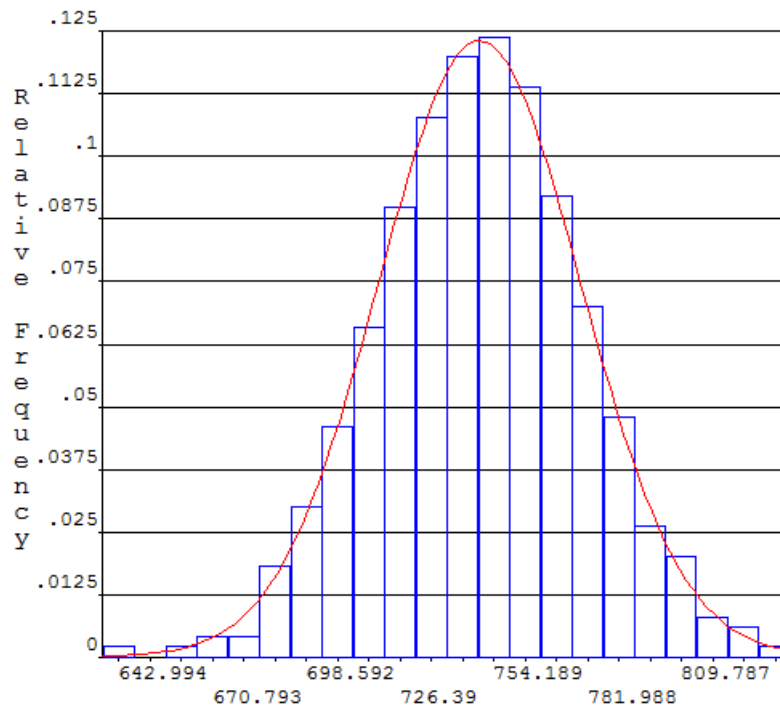


Figure 6.3. The histogram of the yield strength obtained by the Ansys (own source)

From the two figures above we can see that the input parameters follow correctly the given normal distribution for the case of the applied repetition number.

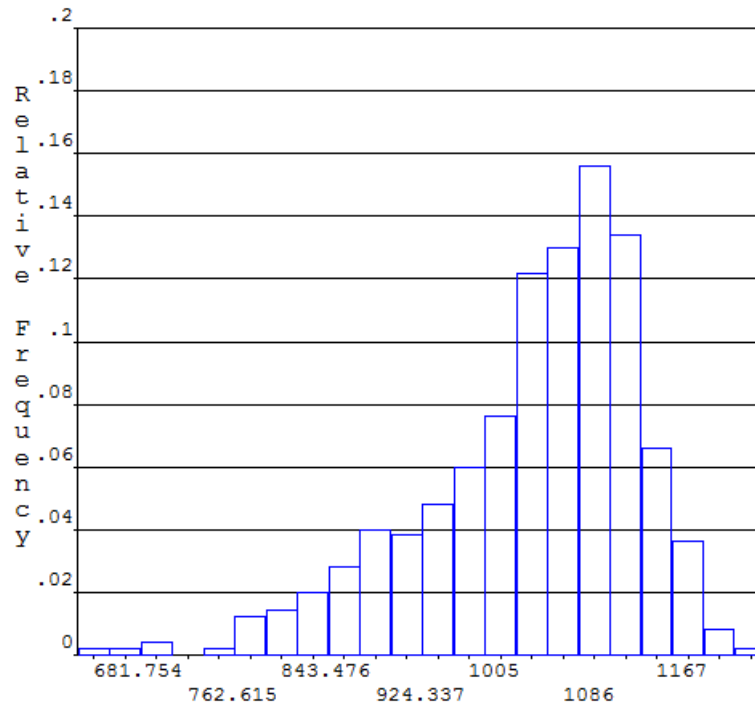


Figure 6.4. The histogram of the axial resistance obtained by the arc-length method in Ansys (own source)

On the last figure, the resistance histogram shows the characteristic shape of the normal distribution, but do not follow it as well as the chord thickness and the yield strength. Practically it means that the obtained results not sufficiently accurate, for that we would need more simulations, but they will not be used for any further purposes, only for the validation.

After the finite element simulation, I perform the Monte-Carlo analysis in *Matlab* for the same repetition number. Now, let us compare the results obtained by *Ansys* and *Matlab*. On the following chart (Table 6.2), beside the received resistances I represent the deviations for the deterministic (it was determined in Chapter 5.2.1, when the modified design formula was created) and stochastic case.

Probabilistic results		Deviation	
$N_{R,FEM}$ [kN]	$N_{R,mod}$ [kN]	Probabilistic	Deterministic
1059,30	1159,60	8,65 %	5,10 %

Table 6.2. Comparison of the different probabilistic results (own source)

The deviation even in the stochastic case is low, but if we compare it with the original deterministic case, it is almost negligible, thus my *Matlab algorithm* has been successfully validated.

6.3. Identification of the safety factor

In this part, firstly I determine the value of the safety factor for the *first assembly* in the *Matlab*, applying very large repetition number and the principles of the Eurocode, after that I summarize the obtained results for all the assemblies in tabulated form. Eventually, I make a suggestion on the final value of this factor.

6.3.1. Partial safety factor for the first assembly

The geometry of the considered assemblies can be found in (*Table 3.1*), and the input stochastic variables in (*Table 6.1*), but of course in this case the mean value of the chord thickness is different. At the Monte-Carlo simulation, in *Matlab* the repetition number is chosen to 100 000, and the *probability density function* of the axial resistance according to the modified formula obtained in this way can be seen on (*Figure 6.5*), which reflects very well the characteristic shape of the normal distribution. At the creation of this function, the *Matlab* firstly represent the histogram of the compression resistance, after that fits a density function to the data.

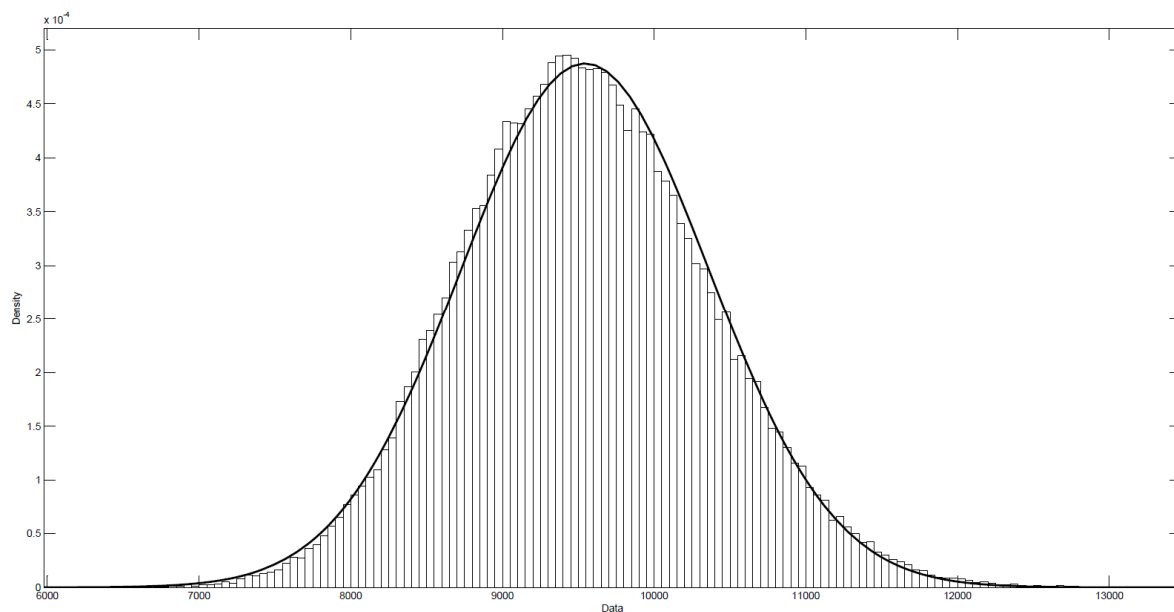


Figure 6.5. The probability density function of the axial resistance for the first assembly (own source)

Before the determination of the safety factor, we must determine the characteristic value of the resistance (at the middle of this function the mean value of the resistance can be found), corresponds to the different assemblies. Generally, the Eurocode prescribe 95 % confidence level for the design values, which means that in the 5 % of the cases it allows the failure due to the different uncertainties (for example the real yield strength of the S690 steel grade is allowed

to be less than 690 MPa in the 5 % of the cases). For the determination of the characteristic resistance I apply the same methodology, so that firstly I represent the *cumulative distribution function*, then calculate the value which corresponds to 0,05. This procedure can be seen on (Figure 6.6).

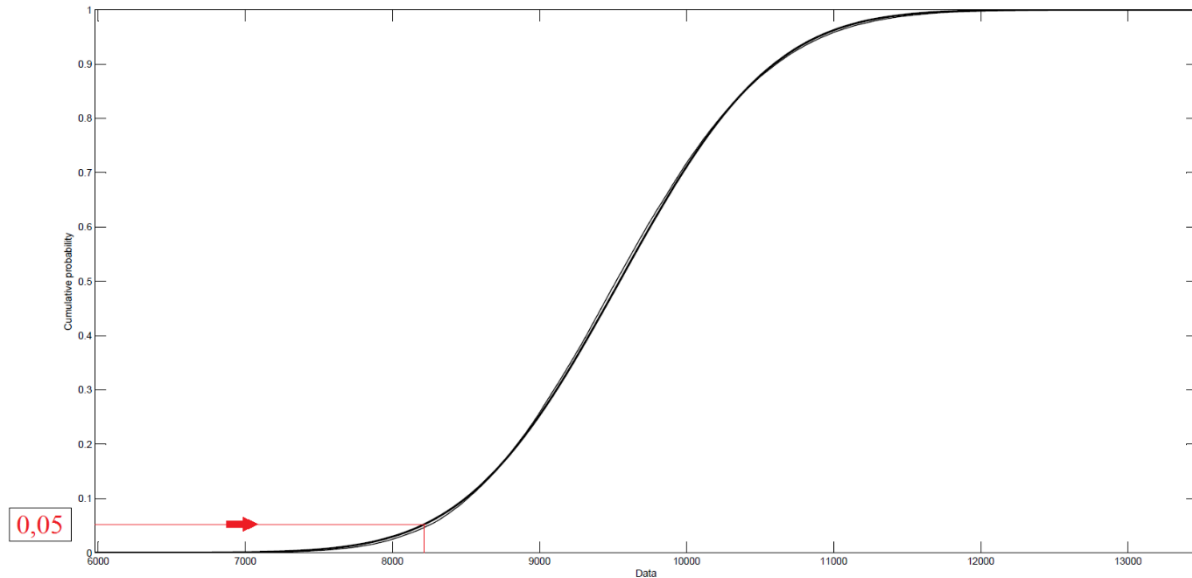


Figure 6.6. Determination of the characteristic value from the distribution function (own source)

For the first assembly, the *characteristic resistance* obtained by this way:

$$N_{R,Char} = 8198,00 \text{ kN} \quad (6.1)$$

The *design resistance* is obtained by using the modified formula with the deterministic value of the chord thickness and yield strength (Table 5.5):

$$N_{R,Design} = 8773,65 \text{ kN} \quad (6.2)$$

Finally, the *safety factor* can be calculated by dividing the design resistance with the characteristic resistance:

$$\gamma = \frac{N_{R,Design}}{N_{R,Char}} = 1,07 \quad (6.3)$$

We can see that in this case the difference is quite small, thus the value of the safety factor is also low, although it corresponds only to the first assembly, and it is not the final value yet.

6.3.1. Tabulated results for all the assemblies

Now, applying the same procedure, I determine the characteristic values and the safety factors for all the assemblies, which are summarized in (Table 6.3).

	$N_{R,Design}$ [kN]	$N_{R,Char}$ [kN]	γ [-]
[1]	8773,65	8198,00	1,07
[2]	6372,49	5396,00	1,18
[3]	4586,10	3581,00	1,28
[6]	5564,10	4449,00	1,25
[7]	3802,85	3438,00	1,11
[8]	2587,21	2339,00	1,11
[10]	2605,11	2179,00	1,20
[11]	1613,20	1352,00	1,19
[12]	1087,02	911,00	1,19
[13]	1642,98	1315,00	1,25
[14]	955,44	765,00	1,25

Table 6.3. The characteristic and design resistances with the safety factors for all the assemblies (own source)

Because these assemblies cover a very large field from the applicable sections, these results can be relevant in the practice. The value of the safety factor varies from 1,07 to 1,28, thus for the benefit of safety this study propose the largest received value, namely:

$$\gamma_{final} = 1,28 \quad (6.4)$$

Finally, let us compare the design values obtained by the modified formula (taking into account the safety factor) and the Eurocode (Table 6.4):

	$N_{Rd,Ec}$ [kN]	$N_{Rd,mod}$ [kN]	$N_{Rd,mod}/N_{Rd,Ec}$ [-]
[1]	6093,29	6854,41	1,12
[2]	4553,97	4978,51	1,09
[3]	3275,47	3582,89	1,09
[6]	3818,18	4346,95	1,14
[7]	2691,34	2970,98	1,10
[8]	1801,64	2021,25	1,12
[10]	1799,57	2035,24	1,13
[11]	1139,39	1260,31	1,11
[12]	729,31	849,24	1,16
[13]	1105,25	1283,58	1,16
[14]	641,16	746,44	1,16

Table 6.4. Comparing the design axial resistances (own source)

Form this table we can see that the obtained design resistances are still above the standard resistances, thus the application of the modified formula leads to more economical design besides keeping the safety prescriptions of the Eurocode.

7. Conclusions

In this study, numerous welded steel T joints made of high strength steel were investigated for axial compression and bending. After a brief review on the design recommendations of the Eurocode, a parametric numerical model was developed in Ansys to determine the load-bearing capacity of the connection, utilizing a very large field of applicable sections with the help of fourteen assemblies. After the convergence test, the successful validation of the finite element was followed, based on the results of a real experiment, and the corresponding validated numerical model. According to the failure mode, a few assemblies were excluded due to the early failure of the member, which overtook the failure of the connection. The results of the materially and geometrically nonlinear numerical simulations implies that the standard design formulae are rather conservative, thus an improvement can be beneficial from economical point of view. With the help of the nonlinear least squares method, new design formulae have been developed by an optimization according to the received results. After obtaining the formulae of the characteristic axial and in plane bending resistance, the determination of the partial safety factor was succeeded. For this purpose, both the material and geometric uncertainties were taken into account in the stochastic model, where at the structural steel as an assumption the stochastic properties of the reinforcing bars were utilized, due to the lack of real test results, thus in the future the experimental investigation of HSS material is really important, to specify the calibration. For one assembly, a Monte-Carlo simulation was performed in Matlab and Ansys. Due to the fact that the results showed sufficient correspondence, henceforth only the Matlab was used to determine the partial safety factors for all cases. After the stochastic simulations, a recommendation on the final value of the safety factor was given. Eventually, the design resistances obtained by the proposed formula and the Eurocode were compared, where the new resistances - besides keeping the adequate level of safety - indicates a more economical design solution, besides the assumptions of this study. In the future, the necessary laboratory investigations on T joints could support the validity of the received results.

8. References

- API. (2005). Recommended Practice for Planning, Designing and Constructing Fixed Offshore Platforms—Working Stress Design. *American Petroleum Institute*.
- Cold Formed Hollow Sections*. (2013). Retrieved from <http://www.consteel.com.sg/downloadfiles/cold%20formed%20hollow%20sections.pdf>
- Eurocode 3 EN 1993-1-1:2005 (E). (2005). Design of Steel Structures. Part 1-1: General Rules and Rules for Buildings.
- Eurocode 3 EN 1993-1-12:2007:E. (2007). Design of Steel Structures. Part 1-12: Additional Rules for the Extension of EN 1993 up to steel grades S700.
- Eurocode 3 EN 1993-1-8:2005 (E). (2005). Design of Steel Structures. Part 1-8: Design of Joints.
- Gogou, E. (2012). Use of High Strength Steel Grades for Economical Bridge Design. *Delft University of Technology*, 90.
- H.S.Mitri. (1988). Ultimate In-Plane Moment Capacity of T and Y Tubular Joints. *J. Construct. Steel Research* 12, 69-80.
- JCCS. (2000). Probabilistic Model Code. Part 3: Material Properties.
- Lesani, M., Bahaari, M., & Shokrieh, M. (2013). Detail Investigation on Un-stiffened T/Y Tubular Joints Behavior Under Axial Compressive Loads. *Journal of Constructional Steel Research*, 91-99.
- SOLID187 Element Description*. (2013). Retrieved from <http://inside.mines.edu/~apetrell/ENME442/Documents/SOLID187.pdf>
- Tata Steel. (2011). Design of Welded Joints.
- Wardenier, J., Kurobane, Y., Packer, J. A., Vegte, A. v., & Zhao, X.-L. (2008). Design Guide for circular hollow section (CHS) joints under predominantly static loading. *CIDECT*.
- Wardenier, J., Packer, J., Zhao, X.-L., & Vegte, G. v. (2010). Hollow Sections in Structural Applications. *CIDECT*.